ЖЭТФ, 2015, том 147, вып. 3, стр. 458–484

FLUX TUBE SPECTRA FROM APPROXIMATE INTEGRABILITY AT LOW ENERGIES

S. Dubovsky [a*], ***R. Flauger*** [a,b], ***V. Gorbenko*** [a]

[a] *Center for Cosmology and Particle Physics Department of Physics, New York University 10003, New York, USA*

[b] *School of Natural Sciences, Institute for Advanced Study 08540, Princeton, USA*

Received September 30, 2014

We provide a detailed introduction to a method we recently proposed for calculating the spectrum of excitations of effective strings such as QCD flux tubes. The method relies on the approximate integrability of the low-energy effective theory describing the flux tube excitations and is based on the thermodynamic Bethe ansatz. The approximate integrability is a consequence of the Lorentz symmetry of QCD. For excited states, the convergence of the thermodynamic Bethe ansatz technique is significantly better than that of the traditional perturbative approach. We apply the new technique to the lattice spectra for fundamental flux tubes in gluodynamics in $D = 3+1$ and $D = 2+1$, and to k-strings in gluodynamics in $D = 2+1$. We identify a massive pseudoscalar resonance on the worldsheet of the confining strings in $SU(3)$ gluodynamics in $D = 3+1$, and massive scalar resonances on the worldsheet of $k = 2, 3$ strings in $SU(6)$ gluodynamics in $D = 2+1$.

Contribution for the JETP special issue in honor of V. A. Rubakov's 60th birthday

DOI: 10.7868/S0044451015030088

1. INTRODUCTION

String theory originated as a candidate theory of strong interactions [1]. However, it was soon abandoned as a theory of hadrons, at least for the time being, because it failed to reproduce the observed properties of deep inelastic scattering as well as the asymptotic freedom of non-Abelian gauge theories. But the success of the Veneziano amplitude in describing many aspects of the hadron spectrum and scattering is hardly a coincidence. Confining strings (flux tubes) are crucial ingredients in the strongly coupled QCD dynamics responsible for color confinement, and their presence is vividly revealed by lattice QCD simulations [2][1)], suggesting that understanding the structure and dynamics of QCD flux tubes might provide insights into the dynamics of color confinement.

The modern approach to the relation between string theory and gauge theories relies on the AdS/CFT correspondence [3]. Within this framework, the QCD flux tube is expected to be described by a string propagating in a space–time with an extra curved dimension, which can be interpreted as the dynamical string tension, or equivalently, the renormalization group scale [4]. Identifying a concrete string theory that would provide a holographic description of nonsupersymmetric QCD remains a long shot, and even if this dual string theory were found, it would be outside the regime in which we currently have theoretical control.

In this paper, we therefore focus on a rather direct path towards understanding the structure of the flux tube theory that does not involve holography. Instead, it is based on existing lattice techniques combined with effective field theory and tools from integrability.

Advances in lattice QCD simulations have allowed measuring the spectrum of low-lying worldsheet excitations with impressive accuracy [5–7]. But the theoretical interpretation of these results was problematic until now. For most states, the string lengths accessible in the lattice simulations were too short for the existing techniques to be reliable. The conventional perturbative methods [8–10] for calculating the spectrum of string excitations result in badly diverging asymptotic

*E-mail: sergei.dubovsky@gmail.com

1) See http://www.physics.adelaide.edu.au/theory/staff/leinweber/VisualQCD/Nobel/ for animations.

series in this regime, preventing the interpretation of the data. At the same time, the data exhibited a number of puzzling and suggestive features. In particular, while perturbative calculations were not reliable, many of the levels show surprisingly good agreement with the spectrum of a free bosonic string quantized in the light-cone gauge following the classic paper [11] by Goddard, Goldstone, Rebbi, and Thorn (GGRT) (see also [12]). This is confusing, given that the GGRT spectrum is well known to be incompatible with the bulk Poincaré symmetry if the number of space–time dimensions is different from 26.

For the lattice simulations, the computational cost grows exponentially with the length of the string. At least with the current technology, this makes it essentially impossible to push lattice calculations into the regime in which conventional perturbation techniques converge. Alternative techniques for calculating the flux tube spectra are thus required, to provide better convergence for relatively short strings. We proposed such a technique in [13], and its success relies on the observation that the worldsheet theory becomes integrable at low energies. This technique seems sufficient to explain the previously puzzling features seen in lattice results. In addition, it allowed showing that the existing lattice data provide strong evidence for the existence of a massive pseudoscalar state on the worldsheet of the QCD flux tube, the worldsheet axion.

The goal of this paper is to provide a detailed account of the method proposed in [13]. In Sec. 2, we begin with a brief summary of the lattice results and of the effective string theory approach (for a detailed recent review, see [14]). We review the results of the conventional perturbative expansion for energy levels, which exhibits a large number of universal terms. We explain that the GGRT spectrum, in spite of being inconsistent with the bulk Poincaré symmetry, still represents a finite-volume spectrum of a certain integrable relativistic *two-dimensional* theory. As we explain, this observation immediately allows calculating all the universal terms in the spectrum of relativistic effective strings [15].

In Sec. 3, we present the new method for calculating the flux tube spectrum. The main idea of the method is to divide the calculation into two steps. First, we perturbatively calculate the worldsheet S-matrix describing the scattering of the flux tube excitations within the effective string theory. We then determine the corresponding finite-volume spectrum using the excited state thermodynamic Bethe ansatz (TBA) [16, 17], which is very similar to the techniques developed by Lüscher [18, 19], which are routinely used to extract four-dimensional scattering amplitudes from the lattice QCD data. We provide a partial diagrammatic interpretation of the perturbative resummation performed by the TBA and explain why it is natural to expect that this method results in a better behaved perturbation theory for excited states.

In Sec. 4, we use this technique to interpret the lattice data. We provide more details than in [13] as to how to implement the method and include a larger set of excited states in our analysis. This extended analysis confirms the conclusion reached in [13]: the lattice data provides strong evidence for the existence of a pseudoscalar state bound to a confining string. We also apply the technique to the available data for three-dimensional gluodynamics. There, we find no evidence for any massive excitations on the fundamental flux tube, but identify massive scalar excitations on k-strings.

We conclude in Sec. 5 by discussing future directions and prospects. We also present an intriguing hint for the existence of additional light bound states, coming from the precision ground-state data.

2. LATTICE DATA VERSUS CONVENTIONAL PERTURBATIVE EXPANSION

We start with a brief summary of lattice results for the excitation spectrum of confining flux tubes. A detailed description of these results and techniques can be found in [5–7] (for a review, see [20]). In most of our discussion, we assume the space-time dimension $D = 4$. However, we also apply our techniques to the available $D = 3$ data. We are interested in the internal dynamics of a single closed flux tube, rather than in effects coming from its boundaries and from interactions between several flux tubes. To discuss these separately, it is necessary to suppress processes where the flux tube can break. This is achieved by performing simulations in pure gluodynamics without dynamical quarks. Gauge-invariant operators in a pure glue theory are constructed as traces of path-ordered exponentials of the gauge field A_μ (Wilson loops),

$$\mathcal{O}_P = \operatorname{Tr} P \left(\exp \int\limits_C A \right), \tag{1}$$

where C is a closed path. In what follows, we mostly discuss flux tubes carrying a single unit of fundamental flux. This amounts to taking the trace in (1) in the fundamental representation of the gauge group.

A nice trick, which allows concentrating on the dynamics of long flux tubes, is to use the nontrivial lattice

topology. Namely, we consider states created by operators of form (1), such that the corresponding path winds around one of the lattice dimensions. It is convenient to think about the corresponding direction as a spatial one, although, of course, all directions on the lattice are Euclidean anyway. States of this kind are orthogonal to conventional glueball states created by operators (1) with contractible paths. This follows from a global Z_N symmetry (center symmetry) present in the $SU(N)$ Yang–Mills theory compactified on a circle. It is generated by gauge transformations such that the corresponding gauge functions satisfy twisted boundary conditions. The twist is performed using a multiplication by an element from the center of the gauge group,

$$g(R) = e^{2\pi ki/N} g(0), \tag{2}$$

where k is an integer.

Transformations satisfying boundary condition (2) act properly on the gauge configurations and preserve the action functional, but do not originate from a well-defined gauge function. Hence, they should be considered as generating a global, rather than gauge, symmetry. Any two transformations with the same twist k are equivalent up to a conventional gauge transformations, and hence the resulting symmetry group is Z_N. A state created by operator (1) with a winding number k carries charge k with respect to this symmetry, and therefore the full Hilbert space splits into a direct sum of N orthogonal subspaces labeled by corresponding winding number (modulo N).

Most of the lattice data discussed here is extracted from the two-point correlators of the states carrying a unit charge under the center symmetry (a brief discussion of k-strings with larger values of the charge is presented in Sec. 4.6). These states represent closed flux tubes with a unit winding number around the compact direction. Considering a large enough set of shapes of the Wilson lines allows probing not only the ground state but also the low-lying excitations of the flux tubes. By measuring the exponential fall-off of the correlators, we extract energies of the states created from the vacuum by the corresponding operators, in the same way as for conventional glueball mass measurements.

A theoretical framework for perturbative calculations of these energies from first principles is provided by effective string theory. The idea is that the flux tube states whose excitation energy above the ground state in the $k = 1$ sector is smaller than the mass of the lightest glueball are described by a two-dimensional effective field theory. In the absence of additional symmetries (such as supersymmetry), the only massless degrees of freedom in this theory are Goldstone modes describing the spontaneous breaking of the bulk Poincaré group $ISO(1, D-1)$ to a residual symmetry group, which remains unbroken in the presence of an infinite straight string. The latter is the product of the worldsheet Poincaré symmetry $ISO(1,1)$ with the transverse rotations $O(D-2)$. This symmetry breaking pattern implies the presence of $D-2$ massless Goldstone degrees of freedom represented by scalar fields X^i. Geometrically, they parametrize transverse excitations of a flux tube, such that its embedding into the bulk space is given by

$$X^\mu = (\sigma^\alpha, X^i),$$

where σ^α $(\alpha = 1, 2)$ are the worldsheet coordinates.

The effective action is constructed as a sum of local geometric invariants corresponding to this embedding, and starts with a Nambu–Goto (NG) term

$$\begin{aligned} S_{string} &= -\ell_s^{-2} \int d^2\sigma \sqrt{-\det h_{\alpha\beta}} + \ldots = \\ &= \ell_s^{-2} \int d^2\sigma \left(-1 - \frac{1}{2}\partial_\alpha X^i \partial^\alpha X^i - \frac{1}{8}\left(\partial_\alpha X^i \partial^\alpha X^i\right)^2 + \right. \\ &\qquad \left. + \frac{1}{4}\left(\partial_\alpha X^i \partial_\beta X^i\right)^2 + \ldots \right), \end{aligned} \tag{3}$$

where

$$h_{\alpha\beta} = \partial_\alpha X^\mu \partial_\beta X_\mu \tag{4}$$

is the induced metric on the worldsheet, ℓ_s is the string scale, and $\ldots$ stands for higher-order terms.

Within this formalism, the problem of calculating the spectrum of low-lying flux tube excitations becomes the computation of the spectrum of low-lying Kaluza–Klein (KK) modes of this two-dimensional effective theory upon compactification on a spatial circle of circumference R. The traditional approach to this problem is a perturbative expansion in powers of ℓ_s/R. One perturbatively calculates the spectrum of a quantum mechanical Hamiltonian obtained after KK decomposition of effective action (3). At any finite order in the ℓ_s/R-expansion, only a finite number of terms from (3) contribute. The procedure is straightforward, even though the algebra may become rather messy in calculating subleading terms in this expansion. The major subtlety in this approach is to enforce the invariance under nonlinearly realized bulk Lorentz transformations at each order of the expansion,

$$\delta_\epsilon^{\alpha i} X^j = -\epsilon(\delta^{ij}\sigma^\alpha + X^i \partial^\alpha X^j), \tag{5}$$

where ϵ is an infinitesimal parameter of the boost/rotation. By construction, classical action (3) enjoys this symmetry, but depending on the regularization scheme, it may be broken at the intermediate stages of the calculation.

As we can see from (3), a large number of terms in the effective action are fixed as a consequence of nonlinearly realized Lorentz transformations (5). Hence, several leading-order terms in the ℓ_s/R expansion are universal and can be predicted in a model-independent way in any D-dimensional theory, giving rise to effective string-like objects. The only assumptions entering this prediction are that the bulk theory is relativistic, has a gap, and the space-time Goldstones X^i are the only massless degrees of freedom carried by the string worldsheet. One example of a leading-order nonuniversal term in effective action (3) that does not vanish on-shell[2)] and is compatible with (5) is

$$\delta S \propto \ell_s^2 \int d^2\sigma \left(\partial_\alpha \partial_\beta X^i \partial^\alpha \partial^\beta X^i\right)^2 .$$

These terms originate from local geometric invariants, such as R^2 and $R_{\alpha\beta}^2$, where $R_{\alpha\beta}$ is the induced curvature of the worldsheet metric. Power counting demonstrates that this term contributes to the spectrum at the order ℓ_s^6/R^7, and hence all the terms up to ℓ_s^4/R^5 are universal. A brute force calculation of all the universal terms is tedious, however, and has not been performed yet. Shortly, following [15], we will review a shortcut that allows obtaining all the universal ℓ_s^4/R^5 terms bypassing a direct calculation.

Confronting the effective string theory predictions with lattice data for $D = 4$ $SU(3)$ gluodynamics leads to several puzzles, as can be seen from Figs. 1, 2, and 3. The data points on these plots represent string energies as a function of the compactification size R. Figure 1 shows the ground-state energies, Fig. 2 shows states with a single left-moving phonon with different values of the KK momentum, and Fig. 3 shows a state with one left-moving and one right-moving phonon, each with one unit of KK momentum. In the last case, different colors label different two-particle states, classified according to representations of the $O(2)$ group of unbroken rotations in the transverse plane.

In addition, we present two theoretical expectations of how these energies might look like. Dotted lines show the sum of universal ℓ_s^4/R^5 effective string theory terms. As explained above, these follow from the consistent first-principle calculation and should agree with the data for sufficiently long strings.

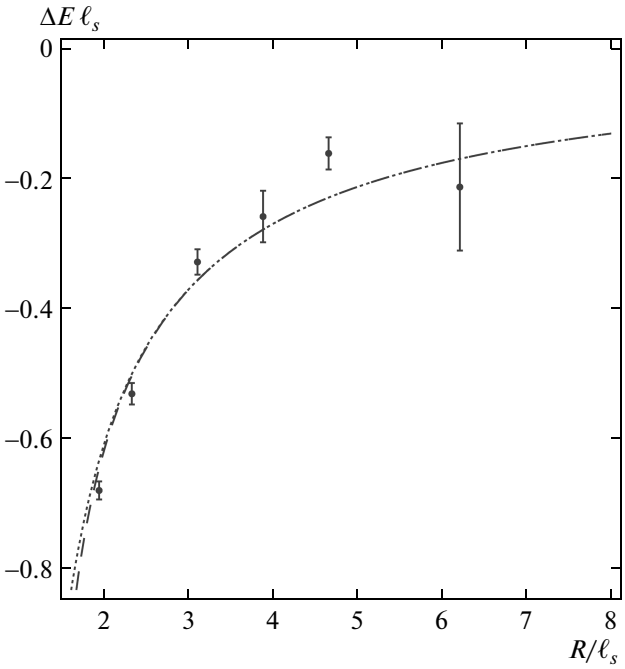

Fig. 1. $\Delta E = E - R/\ell_s^2$ for the ground state of the flux tube. The value of ℓ_s was determined from the lattice data. The dotted line shows the prediction of a derivative expansion. The dashed line shows the prediction of the GGRT theory

The second set of theoretical curves, shown as dashed lines, is an *ad hoc* spectrum, which is traditionally referred to as the "free string spectrum" in the lattice community, following [12]. It is obtained by applying the light-cone quantization method of [11] to a free bosonic string at $D = 4$,

$$E_{LC}(N,\tilde{N}) = \\ = \sqrt{\frac{4\pi^2(N-\tilde{N})^2}{R^2} + \frac{R^2}{\ell_s^4} + \frac{4\pi}{\ell_s^2}\left(N+\tilde{N}-\frac{D-2}{12}\right)}. \quad (6)$$

Here, R is the length of the string, and N and $\tilde{N}$ are levels of an excited string state, such that $2\pi(N-\tilde{N})/R$ is the total KK momentum of the state. In what follows, we refer to this spectrum as the GGRT spectrum. It is not expected to match the spectrum of the QCD flux tube. Indeed, as discussed above, nonlinearly realized Lorentz symmetry imposes strong constraints on the properties of QCD strings. The light-cone quantization is famously incompatible with the target-space Poincaré group away from the critical dimension $D = 26$[3)]. Hence, *a priori*, one might only ex-

[2)] Or, equivalently, cannot be removed by a field redefinition.

[3)] Another interesting exception is $D = 3$, cf. [21].

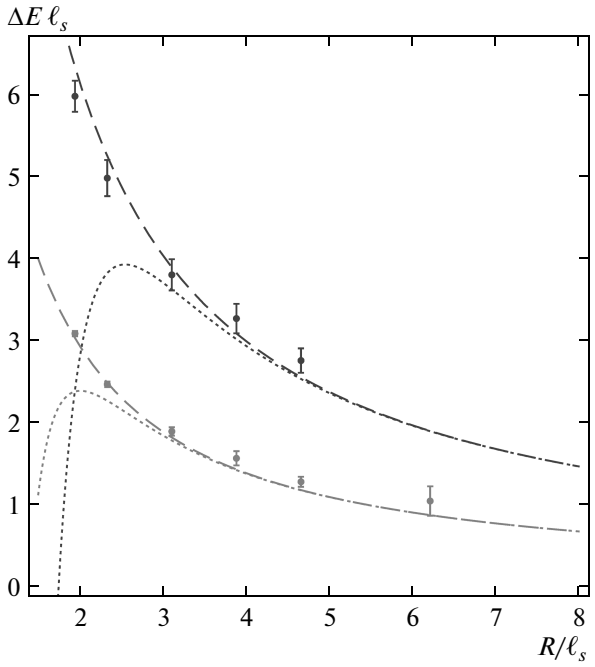

Fig. 2. $\Delta E = E - R/\ell_s^2$ for excited states of the flux tube with one and two units of KK momentum in orange and red, respectively. The dotted lines show the prediction of a derivative expansion. The dashed lines show the prediction of the GGRT theory (color online [37])

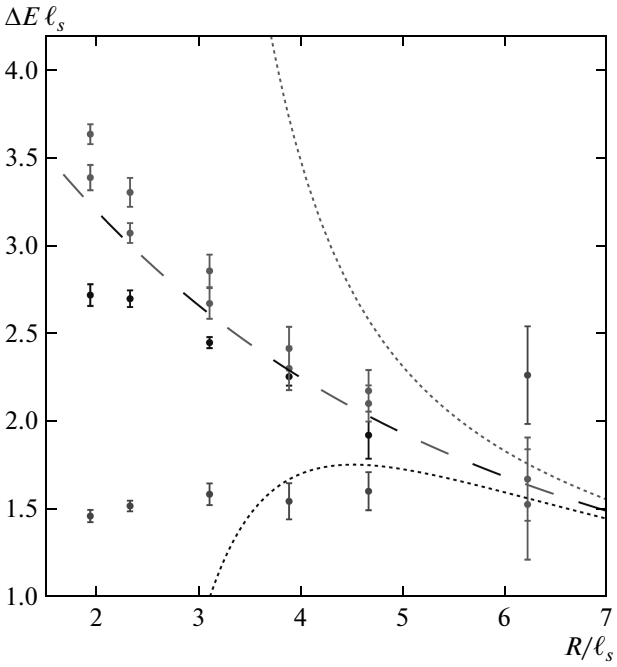

Fig. 3. $\Delta E = E - R/\ell_s^2$ for an excited state with one left- and one right-mover, each with one unit of KK momentum. The dotted lines show the prediction of a derivative expansion. The dashed lines show the prediction of the GGRT theory. The green color represents a state that is a symmetric tensor with respect to $SO(2)$, the blue color represents the states that are scalar with respect to $SO(2)$, and the red data points represent the antisymmetric tensor with respect to $SO(2)$. All states are predicted to be degenerate in the GGRT theory. In the derivative expansion, the scalar and the antisymmetric tensor are still predicted to be degenerate, as indicated by the blue dotted line. The degeneracy with the symmetric state is lifted, which is predicted to have higher energies, as shown by the green dotted line (color online [37])

pect an agreement with a classical limit of the GGRT spectrum in the regime in which the quantum effects can be neglected.

Nevertheless, as seen from Figs. 1–3, the GGRT spectrum surprisingly fits the lattice data better than the perturbative calculations. In fact, the situation is somewhat different for different classes of states. For the ground state, Fig. 1, both the perturbative calculations and the GGRT spectrum agree with each other and with the data even for the shortest strings. This is already a surprise, given that the agreement holds even for strings as short as $R = 2\ell_s$.

For the purely left-moving states, Fig. 2, perturbative calculations agree with the GGRT spectrum and with the data for relatively long strings. For shorter strings, the perturbative expansion breaks down and the data follow the GGRT prediction.

Finally, for the state with both left- and right-moving phonons, Fig. 3, the perturbative expansion is practically useless in the range of the string length for which lattice data are available. The GGRT approximation provides a reasonable approximation for some of the states (the scalar and symmetric tensor), while others (the pseudoscalar) are not explained at all.

These observations taken together provide strong motivation to set up an alternative perturbative expansion with better convergence properties. As a first step, it is desirable to understand the physical origin of the GGRT spectrum for $D \neq 26$. As presented at the moment, it only has the status of an *ad hoc* fitting formula.

The answer to this question was given in [15, 22]. For any value of D, GGRT formula (6) provides an exact answer for the finite-volume spectrum of a certain integrable reflectionless relativistic two-dimensional theory. The exact S-matrix of this theory is determined by a two-particle scattering phase shift of the form

$$\exp(2i\delta_{GGRT}) = \exp(i\ell_s^2 s/4). \quad (7)$$

The special role of the critical dimension $D = 26$ (and also of $D = 3$ [21]) is that in this case, the theory is both integrable and enjoys a nonlinearly realized target-space Poincaré symmetry $ISO(1, D-1)$. The existence of this family of integrable models is not surprising, given that the light-cone string quantization provides a direct canonical construction of the corresponding Hilbert space, and does not break the two-dimensional part of the Poincaré algebra. However, Lorentz invariance had not been firmly established prior to [15, 22][4]. The subtlety is that the conventional light-cone quantization is performed in the sector with zero winding number, while the spectrum (6) arises in the sector with a nontrivial winding. The normal-ordering constant in the light-cone quantization (which determines the $(D-2)$-term in (6)) is usually fixed by imposing the target-space Poincaré symmetry, and it remains unclear what fixes it in the noncritical dimension.

These questions are resolved by applying the TBA method to reconstruct the finite-volume spectrum from the S-matrix in (7). This exactly reproduces the GGRT spectrum (6), both demonstrating that the GGRT spectrum is indeed the finite-volume spectrum of a relativistic two-dimensional theory and showing that the normal-ordering constant is in fact fixed from the requirement of a two-dimensional Poincaré symmetry alone in the sector with a nontrivial winding.

This observation turns out to be important for the idea behind the method described in this paper, and to illustrate its power, following [15], we review how it allows deriving the universal part of the flux tube spectrum in the conventional ℓ_s/R expansion in a simple way. By straightforward perturbative calculation of the scattering amplitudes, we find that at the level of the Lagrangian, the relation between the integrable family of GGRT theories and the effective theory on the worldsheet of an infinitely long relativistic flux tube takes the form

$$\mathcal{L}_{GGRT} = \mathcal{L}_{NG} + \mathcal{L}_{PS} + \dots \quad (8)$$

Here, $\mathcal{L}_{GGRT}$ stands for the Lagrangian of the GGRT theory (determined by the S-matrix in (7)), $\mathcal{L}_{NG}$ is the Lagrangian of the relativistic flux tube theory,

$$\mathcal{L}_{PS} = \frac{D-26}{192\pi}\partial_\alpha\partial_\beta X^i \partial^\alpha\partial^\beta X^i \partial_\gamma X^j \partial^\gamma X^j + \dots \quad (9)$$

is the Polchinski–Strominger (PS) operator [23], and ... stands for higher-order terms in the ℓ_s-expansion. Upon compactification on a circle of circumference R, the infinite-volume relation (8) implies that up to the order $(\ell_s/R)^3$, the flux tube spectrum coincides with the expansion of the GGRT spectrum. The leading $(\ell_s/R)^5$-difference between the two is given simply by the matrix elements of the PS operator. This is the fastest way to derive the universal perturbative ℓ_s/R-results presented in Figs. 1–3. This general argument agrees with the explicit calculations [24] performed for a large set of states in the conformal gauge.

In fact, the flux tube spectrum exhibits an even larger set of universal relations. Relation (8) is a consequence of the universality of the one-loop two-to-two scattering amplitude on the worldsheet of the relativistic flux tube. Power counting demonstrates that actually arbitrary connected one-loop amplitudes are universal and determined solely by the NG part of the action. At a finite volume, this universality translates into relations between energies of different flux tube excitations at higher orders in the ℓ_s/R-expansion. This can be checked by inspecting the leading corrections to binding energies of different states.

Unfortunately, as discussed above, in spite of this high degree of universality, the conventional ℓ_s/R-expansion is not very useful for the study of the excited flux tube states observed in current lattice simulations, which brings us to the main subject of this paper, the description of an alternative technique based on the TBA.

3. FINITE-VOLUME SPECTRA FROM INFINITE-VOLUME SCATTERING

To find a cure for the bad convergence property of the ℓ_s/R-expansion, we first understand the physical origin of the problem. Why do excited states behave so much worse than the ground state, for which the expansion works extremely well? The difference between the ground state and the excited states is visible already in the GGRT theory. As is apparent from expression (6) for the GGRT spectrum, the ℓ_s/R-expansion for excited states breaks down when $R^2/\ell_s^2 \sim 4\pi(N+\tilde{N})$, which can be a relatively large number. For the ground state, however, the radius of convergence corresponds to $R^2/\ell_s^2 = (D-2)\pi/3$, which is much smaller. Physically, the origin of additional terms of the order $2\pi N/R$ in the excited states energies is clear. These are the momenta of free phonons comprising the excited state. This suggests that it is useful to think of the finite-volume energies to be functions of the form

$$E = \ell_s^{-1}\mathcal{E}(p_i\ell_s, \ell_s/R),$$

[4] We thank Ofer Aharony and Zohar Komargodski for emphasizing this point to us.

where p_i are the momenta of individual particles propagating on the worldsheet. The conventional ℓ_s/R expansion assumes the free theory answer for p_i and expands the resulting function in ℓ_s/R. The key idea of the new method is to calculate the spectrum in such a way that these two functional dependences become disentangled.

Our previous discussion, most notably the definition of the GGRT theory by its scattering phase shift (7), suggests a natural language to achieve this. We should perform the calculation of the finite-volume spectrum in two distinct steps: first calculate the (infinite-volume) S-matrix and then proceed towards extracting the finite-volume spectrum from this S-matrix. The first step corresponds to the perturbative expansion in $p_i\ell_s$ and because of the usual analytic properties of the S-matrix turns out to be convergent even for momenta that are not particularly small.

Even though it is widely believed that the S-matrix of a quantum field theory uniquely determines its finite-volume properties, the prescription for the second step is not known in general. However, it is understood in two circumstances.

For massive theories below the particle production threshold, there is a perturbative procedure first implemented by Lüscher [19] and commonly used in lattice calculations. There is no principal obstruction to extending this technique above the inelastic threshold, and multichannel generalizations of Lüscher formulas are being developed (see, e. g., [25, 26]). One of the major challenges (at least at the technical level) within this approach is to calculate winding corrections, coming from virtual particles traveling around the compact dimension. In massive theories, these are exponentially suppressed, and usually are either neglected or calculated by accounting for the lowest-order winding contributions. In a massless theory, like the effective string theory, more care is needed because the winding corrections are only power-law suppressed.

For two-dimensional integrable theories, there is an exact (nonperturbative) method for calculating the finite-volume spectrum known as the TBA [16, 17]. Even writing the complete set of equations, especially for excited states, is in general quite nontrivial and usually involves some amount of guesswork. However, there is a special class of reflectionless integrable scattering, where the TBA for excited states appears to take a simple universal form [22, 27]. The GGRT model belongs to this class and the corresponding set of excited-state TBA equations is known exactly.

The worldsheet theory of flux tubes does not have a mass gap and is not integrable. However, its leading-order scattering amplitudes (in the $p\ell_s$ expansion) coincide with those of the GGRT theory. At the next-to-leading order, relativistic effective strings deviate from the GGRT theory for general D, and reflections and annihilations appear at this order. But in $D = 4$, they still take a special form for which it is possible to write the full set of excited-state TBA equations. This is our starting point for the analysis of the flux tube spectra observed on the lattice. As we see in what follows, this method provides much better control of the spectra than the conventional ℓ_s/R expansion, and makes it clear that the minimal effective string theory has to be extended to explain the lattice data. The extension it to be incorporated in the TBA equations perturbatively.

3.1. Thermodynamic Bethe ansatz for reflectionless scattering

We review the basics of the TBA. For now, we consider massless theories with integrable reflectionless S-matrices with any number of particle species. By integrability, we mean that in every scattering process the number of particles is conserved, the final particles have the same momenta as the initial ones, and the absence of reflections implies that the final distribution of flavors coincides with the initial one. Integrability implies that the S-matrix element for scattering of n left- and m right-moving particles is equal to the product of $n \times m$ pairwise S-matrices. Every $2 \to 2$ S-matrix element in every flavor channel must be just a number with the absolute value 1, as demanded by unitarity,

$$S_{ab}^{cd} = \delta_a^c \delta_b^d \exp(2i\delta_{ab}).$$

The TBA allows extracting the finite-volume spectrum of the theory from the phase shifts δ_{ab}. There are three key ideas underlying this method. The first is called the asymptotic Bethe ansatz (ABA). It is a set of algebraic equations that gives the spectrum in the approximation where the contributions from virtual particles traveling around the "world" are neglected. The ABA equations are discussed in more detail in Sec. 3.2 together with their derivation.

The second idea is the following: instead of considering the theory in a finite volume R and at zero temperature, we consider the theory in which time and space directions are interchanged. Consequently, this theory appears to live in an infinite volume but at a finite temperature $T = 1/R$. For a relativistic theory, the space–time-interchanged ("mirror") theory coincides with the initial one. The ABA becomes exact in the thermodynamic limit and takes the form of certain

integral equations that allow finding the free energy density $f(T)$ in the mirror interchanged theory. The functional integral representation of the partition function implies that it is related to the ground-state energy of the initial theory as

$$E_0(R) = Rf(1/R).$$

To calculate the energy of excited states, the third idea is needed. The prescription is to deform the contour in the integral equations used for calculating the ground-state energy in a certain way [17]. Although the derivation of this procedure for the general case is not yet known, there is a rigorous mathematical proof of the resulting TBA equations for certain integrable theories, such as the sinh-Gordon model [27]. For the GGRT theory (the case we are mainly interested in here) rather nontrivial checks were performed [22] to be certain that the method can be safely applied. In addition to this, in Sec. 3.3, we provide partial diagrammatic intuition behind the TBA equations.

We now turn to presenting the TBA equations themselves. There are two contributions to the energy of a state in this formalism. First, there are "real" particles, with (positive) momenta equal to p_{li} and p_{ri} for left and right movers present in the state. In addition, there is a "thermal bath" of particles with pseudo-energies $\epsilon_l^a(q)$ and $\epsilon_r^a(q)$ for left- and right-moving components of the bath[5)],

$$\Delta E = \sum_i p_{li} + \sum_i p_{ri} + \\ + \frac{1}{2\pi}\sum_a \int_0^\infty dq \ln\left[1-\exp(-R\epsilon_l^a(q))\right] + \\ + \frac{1}{2\pi}\sum_a \int_0^\infty dq \ln\left[1-\exp(-R\epsilon_r^a(q))\right]. \quad (10)$$

The thermal bath contribution is responsible for winding corrections and indeed has a thermal origin from the standpoint of the mirror theory. To distinguish thermal particles from the real ones, we let the momenta of the former be denoted by q. The index a labels a flavor. The momenta p_i label the state. The case without real particles naturally corresponds to the vacuum state.

The real particle momenta p and the pseudo-energies $\epsilon(q)$ are determined from solving the TBA set of integral equations. These consist of two groups of equations. First, there are generalized quantization conditions for the real momenta

$$p_{li}R + \sum_j 2\delta_{a_i a_j}(p_{li}, p_{rj}) - \\ - i\sum_b \int_0^\infty \frac{dq}{2\pi}\frac{d\,2\delta_{a_i b}(ip_{li}, q)}{dq} \times \\ \times \ln\left[1-\exp(-R\epsilon_r^b(q))\right] = 2\pi N_i, \quad (11)$$

$$p_{ri}R + \sum_j 2\delta_{a_j a_i}(p_{ri}, p_{lj}) + \\ + i\sum_b \int_0^\infty \frac{dq}{2\pi}\frac{d\,2\delta_{b a_i}(-ip_{ri}, q)}{dq} \times \\ \times \ln\left[1-\exp(-R\epsilon_l^b(q))\right] = 2\pi \tilde{N}_i. \quad (12)$$

In the absence of interactions, $\delta = 0$, these reduce to the free theory quantization conditions for a set of particles on a circle. For an interacting theory, the quantization condition is modified for two reasons. First, pairwise interactions between real particles explain the appearance of the corresponding phase shifts in (11), (12) (we explain the origin of this effect in Sec. 3.2 in detail). Second, there are integral contributions that account for winding corrections. Imaginary momenta appearing in (11)–(14) come from performing the double Wick rotation to the mirror theory. However, the crossing symmetry, which in terms of the phase shift can be written as

$$\delta(p_l, -p_r) = \delta(-p_l, p_r) = -\delta(p_l, p_r),$$

guarantees that the equations are actually real. We did not use this to simplify the equations and eliminate the i, because the crossing symmetry is modified in the presence of annihilations, which we discuss below.

Finally, the pseudo-energies satisfy the TBA constraints

$$\epsilon_l^a(q) = q + \frac{i}{R}\sum_i 2\delta_{a b_i}(q, -ip_{ri}) + \frac{1}{2\pi R} \times \\ \times \sum_b \int_0^\infty dq' \frac{d\,2\delta_{ab}(q,q')}{dq'} \ln\left[1-\exp(-R\epsilon_r^b(q'))\right], \quad (13)$$

$$\epsilon_r^a(q) = q - \frac{i}{R}\sum_i 2\delta_{b_i a}(q, ip_{li}) + \frac{1}{2\pi R} \times \\ \times \sum_b \int_0^\infty dq' \frac{d\,2\delta_{ba}(q,q')}{dq'} \ln\left[1-\exp(-R\epsilon_l^b(q'))\right]. \quad (14)$$

[5)] As before, we let the energy be denoted by ΔE, as a reminder that the full energy E in addition contains the classical string tension contribution R/ℓ_s^2.

For the GGRT phase shift $2\delta_{a_ib_j} = \ell_s^2 p_{li} p_{rj}$, it is straightforward to solve the full TBA system (11)–(14) analytically, resulting in (6). We note that in the massive sinh-Gordon model, the full TBA system takes the same form [27], strongly suggesting that this form should be universal for reflectionless scattering. The full set of TBA equations has a rather intimidating appearance, but as we just explained, the major complications come from winding corrections. Dropping them results in the ABA equations, which are known as the Lüscher formula in the context of lattice calculations,

$$p_{l(r)i} R + \sum_j 2\delta_{a_i a_j}(p_{l(r)i}, p_{r(l)j}) = 2\pi N_i. \qquad (15)$$

In the massive case, all integral terms are suppressed as $\exp(-\mu R)$, where μ is the mass gap, as is natural to expect for winding corrections. In our case, the winding corrections are only power-law suppressed, and we have to pay more attention to them. However, as we see in what follows, for the values of R we consider, the main effect still comes from the asymptotic part of the Bethe ansatz. We explain the reason for this in Sec. 3.4.

3.2. Asymptotic Bethe ansatz

In this section, we sketch a simple derivation of the multichannel generalization of the ABA equations. It is certainly not new. One of the reasons to present the ABA derivation here is to stress that the logic underlying this derivation does not directly rely on integrability. In particular, we allow nondiagonal scattering, and hence the amplitude is no longer reflectionless. Conceptually, there appears to be no obstruction to generalizing the ABA to accommodate particle production. For example, to account for the $2 \leftrightarrow 4$ processes, we should add matrix elements mixing two- and four-particle states. In the case at hand, however, these processes are suppressed at low energies. In what follows, we therefore neglect these effects and assume that the $2 \to 2$ part of the S-matrix S_{ab}^{cd} is unitary.

We first consider two particles in an infinite volume, the first one moving to the right and the second moving to the left. The basis for the in-states is formed by $|p_r, a; p_l, b\rangle$ and the wave function of a generic state is defined as

$$\psi^{ab}(x_1, x_2) = \langle 0|\phi^a(x_1)\phi^b(x_2)F^{cd}|p_r, c; p_l, d\rangle, \qquad (16)$$

where the field operators are taken at equal time, F^{cd} denotes the flavor wave function, and we suppressed the time dependence. Strictly speaking, our discussion assumes that the states are taken to be wave packets, but to keep the formulas short, we do not write this explicitly. When particles are far apart, they do not interact with each other, the energy of the state is given by $|p_l| + |p_r|$, and the wave function is just a product of two plane waves. Thus, in the region $x_1 \ll x_2$, the wave function consists of two contributions: either the first particle is found at x_1 and the second at x_2 (before they scattered), or the second particle is found at x_1 and the first at x_2. In the latter case, the particles have to scatter before they reach their positions. As a result, the total wave function in this region takes the form

$$\psi^{ab}(x_1 \ll x_2) = \exp(ip_r x_1 + ip_l x_2)F^{ab} + \\ + \exp(ip_l x_1 + ip_r x_2)S_{cd}^{ba}F^{cd}. \qquad (17)$$

The same reasoning applied in the region $x_1 \gg x_2$ gives

$$\psi^{ab}(x_1 \gg x_2) = \exp(ip_l x_1 + ip_r x_2)F^{ba} + \\ + \exp(ip_r x_1 + ip_l x_2)S_{cd}^{ab}F^{cd}. \qquad (18)$$

Now we consider this state in a finite volume and impose the corresponding periodicity condition. To achieve this, we consider x_1 and x_2 such that $x_1 \ll \ll x_2 \ll x_1 + R$. Then the periodicity of the wave function $\psi(x_1, x_2) = \psi(x_1 + R, x_2)$ requires that

$$\exp(ip_r R)S_{cd}^{ab}F^{cd} = F^{ab}. \qquad (19)$$

All other periodicity conditions are equivalent because the total momentum $p_1 + p_2$ is quantized in units of $2\pi/R$. Equation (19) has solutions if and only if

$$\det\left[\exp(ip_r R)S_{cd}^{ab} - \delta_c^a \delta_d^b\right] = 0, \qquad (20)$$

where (ab) as well as (cd) should be treated as a single matrix index when the determinant is taken. This is the multi-channel generalization of the Lüscher formula, which imposes a relation between the S-matrix and the allowed momenta of particles in a finite volume. If the S-matrix is known, it allows finding the energy spectra, given by $|p_l| + |p_r|$. Conversely, if the spectra as functions of R are known, we can reconstruct the S-matrix.

It is straightforward to extend this derivation to mulitparticle states in integrable theories. In particular, for reflectionless scattering, we immediately arrive at (15). As we already said, there appears no fundamental obstruction to extending these arguments to nonintegrable theories, even though obtaining the explicit equations is likely to be quite challenging due to inevitable mixing between states with different numbers of particles.

Anticipating a discussion in what follows, we point out one of the main reasons why the TBA technique displays better convergence than the conventional (ℓ_s/R) expansion. As follows from ABA equations (15), the actual momenta p_i of interacting phonons are smaller than the free-theory value $2\pi N_i/R$, if the phase shift δ is an increasing function of the momentum. Given that the perturbative parameter for the low-energy expansion is $p_i\ell_s$, accounting for this effect improves the convergence properties of the expansion.

3.3. Towards a diagrammatic interpretation of the thermodynamic Bethe ansatz

It is clear from the presented derivation that the winding corrections are absent in ABA system (20) because we did not take virtual quanta propagating around the world into account. For the GGRT theory, these are accounted for by the "thermal" contributions in (10) and (11), (12) together with a set of integral equations (13), (14) for pseudo-energies.

These equations were obtained following the idea pioneered in [17]. The starting point are the ground-state TBA equations derived in [16]. These are Eqs. (10) and (13), (14) without any real particle contributions. The idea in [17] is that the ground-state energy as a function of a sufficiently large set of external parameters allows reconstructing the full set of excited states energies by analytic continuation in the parameters and exploiting the monodromies the equations and solutions undergo when circling singularities in the complex plane.

To arrive at the excited-state TBA equations for the GGRT model, we can for example introduce chemical potentials $\mu^a_{l(r)}$ for the number of phonons. These are incorporated by shifting the pseudo-energies

$$\epsilon^a_{l(r)} \to \epsilon^a_{l(r)} + \mu^a_{l(r)}$$

in the thermal integrals in (13) and (14). As a result of an analytic continuation along a contour in the complex plane of the μ, which starts and ends at $\mu = 0$, the integrals may pick up extra contributions from circling around the branch points of the logarithm. These give rise to the contributions in (13) and (14) corresponding to real particles. The generalized ABA equations (11), (12) determine the positions of the singularities. The particle number simply counts how many times different singularities were circled.

Unfortunately, there is still an ambiguity left in this prescription concerning the correct direction for circling around the singularities (the one corresponding to positive particle numbers N_i). This may be fixed by requiring that the correct result be reproduced in the free-theory limit, $\ell_s \to 0$.

This line of reasoning leads to the correct result for the excited-state TBA. Nevertheless, it is tempting to look for a diagrammatic understanding of how the excited-state TBA arises. In particular, we may hope to see that it corresponds to a certain resummation of the conventional perturbative expansion, which would help to illuminate the origin of the better convergence of the TBA method. Some insight into this issue was given in [18, 19] (see [28] for a review and generalization to an arbitrary dispersion relation). However, the proposed diagrammatic method corresponds to an expansion in winding corrections or $\exp(-mR)$ because massive particles were considered. Since winding corrections in massless theories are only power-law suppressed, this expansion does not provide a good approximation. This motivates us to seek an alternative resummation of Feynman diagrams.

At this point, we do not have a complete solution to this problem, but instead merely report on partial progress in this direction. First, we recall that even though our theory is massless and winding corrections are not suppressed exponentially, numerically they are nevertheless small for the relevant values of $D-2$. We already mentioned the reason for this at the end of Sec. 3.1 and illustrate this point numerically below. This suggests an iterative solution of the TBA equations, in which we first ignore the integral parts, find the corresponding ϵ and p, and then solve the integral equations iteratively.

We note that this expansion is different from the expansion in the winding number mentioned above. The latter corresponds, roughly, to expanding the thermal TBA logarithms in a series of exponential terms $\exp(-nR\epsilon)$.

To see that the convergence of this method is good at least for the GGRT theory, we note that to the leading order, it corresponds to the expansion of the square-root formula (6) in a formal parameter $D-2$, and that expansion is convergent for any state for the values of R and $D-2$ we consider. For the ground state, the $(D-2)$ expansion is equivalent to the ℓ_s/R expansion, but they behave differently for all excited states. For instance, completely neglecting the $(D-2)$ contributions results in the following ABA spectrum for the GGRT theory:

$$E_{cl}(N,\tilde{N}) = \\ = \ell_s^{-1}\sqrt{\frac{R^2}{\ell_s^2} + \frac{4\pi^2\ell_s^2(N-\tilde{N})^2}{R^2} + 4\pi\left(N+\tilde{N}\right)}. \quad (21)$$

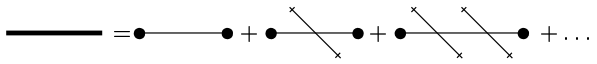

Fig. 4. Propagator for a virtual quantum in the presence of the real left-moving particles indicated by crosses

This coincides with the spectrum of the classical string. In the rest of this section, we demonstrate how the first term of the $(D-2)$ expansion of spectrum (6) arises in the diagrammatic language.

We will organize the calculation in the following way. We start with a set of particles corresponding to a chosen state, with momenta determined by the ABA quantization conditions. At this stage, winding corrections are not yet included, and it is therefore appropriate to think of this state as a "gas" in an infinite volume, albeit in a very special state in which all particles have the same momentum. The leading winding corrections then take the form of conventional bubble diagrams with the propagator taken to be the one for fluctuations around this gas.

To illustrate how this works in practice, we first consider a state on a circle with a single left-moving phonon. The ABA quantization is equivalent to the free one in this case, and hence the momentum of the particles in the gas is $p_l = 2\pi N/R$. It is convenient to also introduce the parameter $\alpha_l = \ell_s^2 p_l/R$; physically, this is the energy density of the gas (in string units). We consider a probe particle with a momentum q_α, propagating through the gas. To calculate the dressed propagator for this particle, we need to resum the diagrams represented in Fig. 4. In terms of the momentum expansion, we restrict ourselves to the leading term; only tree-level diagrams are then taken into account. All one-particle irreducible diagrams containing more than two gas insertions vanish in this case, and we thus obtain the propagator exactly to all orders in α_l as a geometric series,

$$G(q) = \frac{i}{q_0^2 - q_1^2} + \frac{i}{q_0^2 - q_1^2}\,\frac{i\mathcal{M}}{2p_l R}\,\frac{i}{q_0^2 - q_1^2} + \dots, \quad (22)$$

where $\mathcal{M}$ is the forward scattering amplitude for the scattering of the virtual particle off a phonon in the gas,

$$\mathcal{M} = 2\ell_s^2 p_l^2 (q_0 + q_1)^2,$$

and the factor of $1/R$ stands for the number density of phonons. By calculating the geometric series, we obtain

$$G(q) = \frac{i}{(q_0 + q_1)\left[q_0 - q_1 + (q_0 + q_1)\alpha_l\right]}. \quad (23)$$

Since left-movers do not interact with each other, the dispersion relation for a left-moving quantum is not modified in a purely left-moving gas. On the other hand, the right-moving probe is slowed down by interactions and its dressed dispersion relation is

$$q_0 = \frac{1 - \alpha_l}{1 + \alpha_l}\, q_1.$$

We note that for $\alpha_l > 1$, a "right-mover" is carried away by the gas and actually propagates to the left. It is now straightforward to construct the quadratic effective action reproducing propagator (23),

$$S_{eff} = \int d^2\sigma \left(\frac{1+\alpha_l}{2}\dot{x}^i\dot{x}^i + \frac{\alpha_l}{2}\dot{x}^i x^{i\prime} - \frac{1-\alpha_l}{2}x^{i\prime}x^{i\prime}\right). \quad (24)$$

Now, following the logic outlined above, we calculate the energy of the state on a circle as the sum of the energy of the real left-moving particle, p_l, and the winding contribution. In the leading order, the latter is the ground-state energy of the free theory with action (24). It can be calculated either using the ground-state TBA (for the mirror theory) or directly. Proceeding in the direct way, we calculate the energy as the expectation value of the Hamiltonian corresponding to (24),

$$\langle H_{eff}\rangle = \left\langle \int_0^R d\sigma \frac{1+\alpha_l}{2}\dot{x}^i\dot{x}^i + \frac{1-\alpha_l}{2}x^{i\prime}x^{i\prime}\right\rangle. \quad (25)$$

Using the Poisson summation formula, we write the result as a sum over windings,

$$\langle H_{eff}\rangle = \sum_{n\neq 0}\int \frac{d^2q}{(2\pi)^2} \times \\ \times \frac{iR\left((1+\alpha_l)q_0^2 + (1-\alpha_l)q_1^2\right)\exp(iq_1 nR)}{2(q_0+q_1)(q_0 - q_1 + (q_0+q_1)\alpha_l)}, \quad (26)$$

where we drop the zero-winding contribution. After performing the Wick rotation for q_0, we close the q_1-contour and take the q_1-integral by residues. The resulting total energy of the state is

$$\Delta E = p_l + \frac{D-2}{2\pi}\left\{\int_0^\infty dq \ln\left[1 - \exp(-Rq)\right] + \right. \\ \left. + \int_0^\infty dq\,(1-\alpha_l)\ln\left[1 - \exp(-Rq(1+\alpha_l))\right]\right\} = \\ = \frac{2\pi N}{R} - \frac{(D-2)\pi R}{6(R^2 + 2\pi N\ell_s^2)}. \quad (27)$$

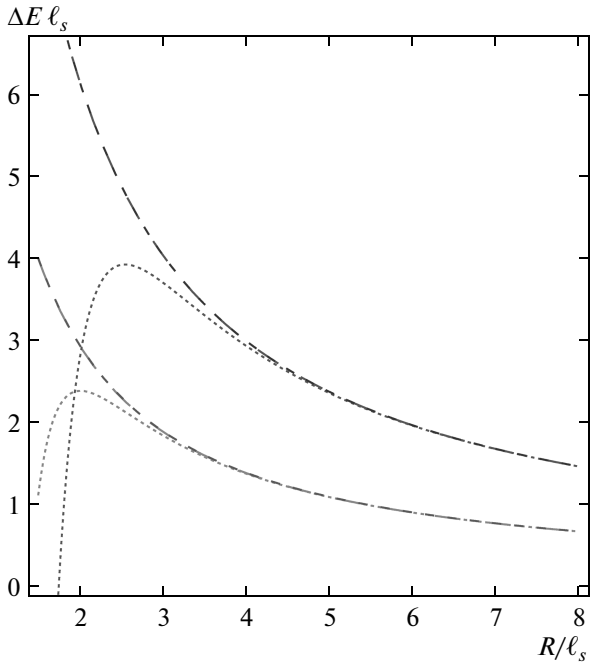

Fig. 5. $\Delta E = E - R/\ell_s^2$ for excited states of the GGRT theory with one and two units of the KK momentum in orange and red, respectively. The dotted lines show the prediction of the derivative expansion, the longer dashes show the prediction of the GGRT theory, and the shorter darker dashes represent our diagrammatic approximation. The diagrammatic approximation and the exact result are virtually indistinguishable (color online [37])

This is exactly the result that follows from the first iteration of solving integral equations (10)–(13) perturbatively in winding contributions, or equivalently by expanding the exact answer (6) in $D-2$. Unlike the ℓ_s/R expansion, approximation (27) provides an extremely accurate estimate for the exact result down to $R \sim \ell_s$ (see Fig. 5).

Furthermore, just like the exact result, expression (27) turns into a series with a rather small radius of convergence, when expanded in ℓ_s/R. The above derivation sheds light on the physical origin of this behavior and on the nature of the improvement achieved by the TBA method. The singularity in (27), which determines the radius of convergence of the ℓ_s/R expansion, corresponds to $\alpha_l = 1$, when both modes become left-movers. Using the dressed propagator in our calculation allows avoiding spurious singularities associated with this effect.

The same reasoning can be applied to all states that contain only left-moving excitations. In principle, there is no obstacle to extend the same logic to the states containing both left- and right-moving phonons. One modification in this case is that the momenta p_l and p_r of the particles in the gas are not given by the free quantization condition anymore, but are solutions of Lüscher equation (15). The difficulty now, however, is how to obtain the result in all orders in the particle energy densities $\alpha_{l(r)} = \ell_s^2 p_{l(r)}/R$. The reason is that left- and right-moving particles now interact with each other, and hence there are nonvanishing one-particle irreducible diagrams with more than four outgoing legs contributing to the dressed propagator. It may be possible to sum all these diagrams for the NG action at least at the tree level, but we leave this for future work. Instead, we present the perturbative result in the α, accounting only for the four-particle interactions, as before. This leads to the following dressed propagator for a probe particle:

$$G(q) = \frac{-i}{q_0^2 - q_1^2 + (q_0^2 + q_1^2)\alpha_l + (q_0^2 - q_1^2)\alpha_r R}. \quad (28)$$

As expected, the dispersion relation for both left- and right-movers is modified in this case. A calculation similar to the one we did for the purely left-moving state results in the following expression for the energy at the leading order in the α:

$$\Delta E = p_l + p_r - (D-2)\frac{\pi\,(1-\alpha_l-\alpha_r)}{6R}. \quad (29)$$

As illustrated in Fig. 6, this leads to a significant improvement compared with the naive ℓ_s/R expansion, but still is not accurate at small radii, where the energy densities $\alpha_{l(r)}$ become large and multiparticle interactions must be included.

We feel the above perturbative examples serve well the purpose of illustrating the physics underlying the TBA method. It is an interesting open question whether they can be pushed to higher orders. We have mentioned that already at the tree level, we must learn how to resum an infinite number of tree-level diagrams. But we may also try to be more ambitious and push the matching calculation resulting in effective action (24) to higher orders. It would be interesting to study whether this method allows reproducing the full TBA system in the $(D-2)$ expansion, or whether new physical ingredients are required.

3.4. UV insensitivity of winding corrections

It is apparent from the above discussions that winding corrections are more subtle and harder to account for than the ABA part of the finite-volume spectrum.

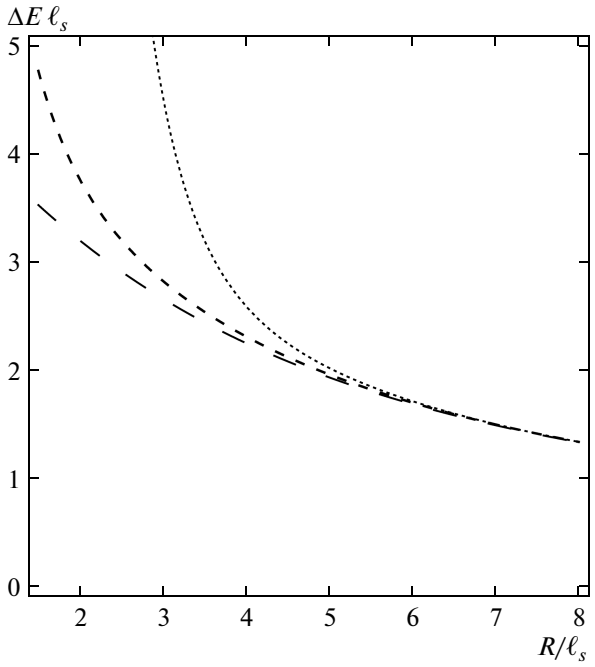

Fig. 6. $\Delta E = E - R/\ell_s^2$ for excited states of the GGRT theory with one left- and one right-moving phonon, each with one unit of the KK momentum. The dotted lines show the prediction of the derivative expansion, the longer dashes show the prediction of the GGRT theory, and the shorter darker dashes represent our diagrammatic approximation

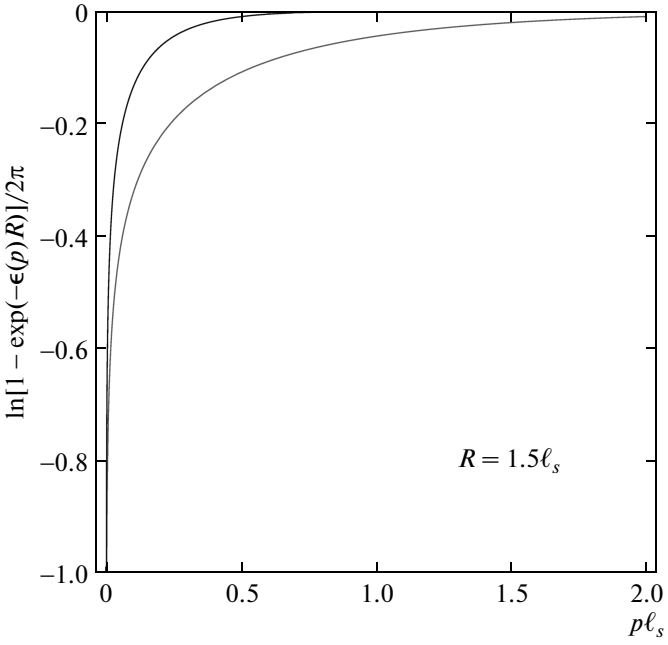

Fig. 7. The integrand appearing in the winding corrections as a function of momentum. The blue line represents the integrand for the ground state. The red line shows the integrand for left-moving pseudo-particles in the presence of a right-moving excitation with one unit of the KK momentum or *vice versa*. The radius of the circle is taken to be $R = 1.5\ell_s$, smaller than the radii we are typicall interested in. Nevertheless, the integral is dominated by soft pseudo-particles and is rather insensitive to the UV behavior of the scattering amplitude (color online [37])

In particular, if one is interested in a specific state with a fixed number of particles, solving the ABA requires diagonalizing the S-matrix only in that sector. On the other hand, accounting for winding corrections always involves a complete diagonalization of the S-matrix for an arbitrary number of particles. Below, when discussing the resonance contribution in Sec. 4.3, we find ourselves in the situation where the ABA part is straightforward to write and solve. At the same time, a complete diagonalization of the S-matrix is currently unavailable, and the winding corrections cannot be accounted for.

In a situation like this in massive theories, it is a common practice to neglect the winding corrections, given that these are now exponentially suppressed. In Sec. 4.3, we follow a similar strategy and use a lower-order approximation for the phase shift in the winding part of the TBA than in the ABA part. Heuristically, this may be justified by noting that the problem arises due to the massive resonant contribution, and the same justification as in the massive case applies. In fact, there is a general reason for winding corrections to be less sensitive to the UV physics than the asymptotic part. The integrals over the thermal bath in the full TBA system are exponentially cut off for momenta above $q \sim 1/R$, which is smaller than the characteristic momenta of real particles. In the free-theory approximation, the latter are of the order $2\pi/R$. We illustrate this point for the GGRT theory in Fig. 7. We see that even for a very short compactification radius, the winding integral is dominated by rather soft momenta and, as a consequence, is not very sensitive to higher-order corrections to the amplitude.

4. ENERGY LEVELS OF FLUX TUBES

We are now in a good position to move on to the main topic of the paper and to apply the TBA technique to the calculation of the flux tube spectra. The first step is to calculate the worldsheet S-matrix pertur-

batively in the $p\ell_s$ expansion. As explained in Sec. 2, the phonon scattering on the worldsheet of a flux tube is universal up to ℓ_s^4. The corresponding amplitudes were calculated in [15]. At this order, there is no particle production, and hence the S-matrix is integrable and completely determined by the two-particle elastic amplitudes. To describe these last, it is convenient to characterize two-particle states according to their quantum numbers under the unbroken group $O(2)$ of rotations in the transverse plane. We find one scalar $|s\rangle$, one pseudoscalar $|p\rangle$, and two components $|t,\pm\rangle$ of the symmetric tensor $O(2)$ representations. Introducing creation operators for states of definite helicity, i. e., eigenstates of the continuous $SO(2)$ rotations in the transverse (X^2, X^3) plane,

$$a^\dagger_{l(r)\pm} = a^\dagger_{l(r)2} \pm i a^\dagger_{l(r)3}, \tag{30}$$

we write the corresponding states in the form

$$\begin{aligned} |s\rangle &= (a^\dagger_{l+}a^\dagger_{r-} + a^\dagger_{l-}a^\dagger_{r+})|0\rangle, \\ |p\rangle &= (a^\dagger_{l+}a^\dagger_{r-} - a^\dagger_{l-}a^\dagger_{r+})|0\rangle, \\ |t,\pm\rangle &= a^\dagger_{l\pm}a^\dagger_{r\pm}|0\rangle. \end{aligned} \tag{31}$$

The two-particle S-matrix is diagonal in basis (31) and in the order ℓ_s^4 reduces to the elastic scattering phases in each of the channels, which are equal to

$$\delta_{s(p)} = \delta_{GGRT} + \delta_{PS} + \mathcal{O}(\ell_s^6), \tag{32}$$

$$\delta_t = \delta_{GGRT} - \delta_{PS} + \mathcal{O}(\ell_s^6), \tag{33}$$

where δ_{GGRT} is the GGRT phase shift (7) and δ_{GGRT} is the PS phase shift given by

$$2\delta_{PS} = \frac{26-D}{24\pi}\ell_s^4 (p_l p_r)^2, \tag{34}$$

where we restored the dependence on the dimension D of the target space-time[6]. The appearance of the critical string dimension $D_c = 26$ in the PS phase shift (34) indicates that it introduces qualitatively new effects as compared to the leading GGRT phase shift. Indeed, it can be shown that the PS phase shift is responsible for the eventual breaking of integrability on the worldsheet of a noncritical string at a higher order in the ℓ_s expansion.

At the order ℓ_s^4, which we are working in, the theory is still integrable, but is not reflectionless anymore. The PS shift removes the degeneracy between phase shifts in different channels; the phase shift in the tensor channel is different from the one in the scalar and pseudoscalar channels. As a consequence, annihilation transitions like $a^\dagger_{l2}a^\dagger_{r2}|0\rangle \to a^\dagger_{l3}a^\dagger_{r3}|0\rangle$ are possible at this order.

As a result, in general, one expects that the reflectionless TBA described in Sec. 3 can no longer be applied. For general D, this is indeed the case. But the case $D = 4$, where the string has only two transverse directions, is special. Switching to the helicity basis (30) allows diagonalizing the S-matrix for an arbitrary number of particles. Hence, for two flavors, we can still apply the full reflectionless excited TBA system described in Sec. 3. The only modification is that the TBA particles have to be labeled by their helicities rather than by $O(2)$ flavors. The corresponding phase shifts are given by

$$\begin{aligned} \delta_{++} &= \delta_{--} = \delta_t, \\ \delta_{+-} &= \delta_{-+} = \delta_{s(p)}. \end{aligned} \tag{35}$$

Before concluding the section, we briefly comment on the $D = 3$ case because we discuss the $D = 3$ lattice data in what follows. In that case, we find a single two-particle state with zero total momentum. The PS amplitude in this case vanishes for kinematic reasons, and the worldsheet S-matrix agrees with the GGRT S-matrix at the order ℓ_s^4.

We now apply the TBA approach to various states (and theories).

4.1. Ground-state energy

As discussed in Sec. 2, the ground state is the only state for which the conventional ℓ_s/R expansion is adequate for explaining the data. The vacuum matrix element of the PS operator in (9) vanishes. Hence, the ground-state energy deviates from that in the GGRT model only at the order $(\ell_s/R)^7$. As shown in Fig. 1, the sum of the universal terms agrees very well with the lattice data. We find equally good agreement by applying the TBA method. Using the leading ℓ_s^2-order expression for the phase shift (i. e., the GGRT phase shift), the solution of the TBA equations with $N = \tilde{N} = 0$ reproduces the GGRT vacuum energy (see [22] for details). Figure 1 shows that the two results are undistinguishable at the currently available level of precision of the lattice data.

Including the PS phase shift does not change the answer, in agreement with the result from the ℓ_s/R expansion. Indeed, in this case, all TBA particles are characterized by a single pseudo-energy $\epsilon(q)$, which is obtained by solving a single TBA constraint that takes

[6] Of course, for $D \neq 4$, expressions (31) should be modified, and the pseudoscalar representation turns into an antisymmetric tensor.

the form (cf. with the general form of the TBA constraints in (13), (14)),

$$\epsilon(q) = q + \frac{1}{2\pi R}\int dq' \left(\frac{d\,2\delta_{++}(q,q')}{dq'} + \right.$$
$$\left. + \frac{d\,2\delta_{+-}(q,q')}{dq'}\right) \ln\left[1 - \exp(-R\epsilon(q'))\right]. \quad (36)$$

The PS contribution cancels in the sum of the phase shifts, and we obtain exactly the same pseudo-energy as in the GGRT theory, and correspondingly the same result for the vacuum energy.

4.2. Purely left(right)-moving states

We turn to states that contain only left- (or right-) moving real phonons, i. e., $\tilde{N} = 0$ and arbitrary N. This is the simplest class of states for which the standard ℓ_s/R expansion breaks down even for relatively long strings, as can be seen in Fig. 2. Fortunately, these states are still simple from the point of view of the TBA. The ABA is especially simple because there are no interactions between left-movers. Accounting for windings by keeping the leading GGRT part of the scattering amplitude, we obtain the GGRT expression as an approximation for the energies of these states. As we already discussed, this approximation works very well.

To find the result for the amplitude to the order ℓ_s^4 given in Eq. (35), we have to solve the TBA constraints (13) and (14) for four different pseudo-energies, $\epsilon_l^{\pm}$ and $\epsilon_r^{\pm}$. As a consequence, different from the ground state, the energies acquire a dependence on the PS phase shift (even though the PS operator has zero matrix elements for these states, and hence there is no $(\ell_s/R)^5$-correction in the standard perturbative expansion). The TBA equations together with the explicit expressions for the phase shifts (35) imply that pseudo-energies are now complex and have the form

$$\epsilon_{l(r)}^{\pm}(q) = c_{l(r)}q \pm i d_{l(r)}q^2 \quad (37)$$

with real $c_{l(r)}$ and $d_{l(r)}$.

The resulting set of equations for the coefficients c and d is straightforward to solve numerically. The result is presented in Fig. 8. The figure shows both the result in which the windings are evaluated for the phase shift at the order ℓ_s^4 as discussed here and for the GGRT phase. In accordance with our earlier discussion about the UV insensitivity of the winding corrections, the effect of the PS phase is very small ($\lesssim 0.5\,\%$).

The GGRT winding corrections are in fact also small. This can be seen in Fig. 8, which also shows

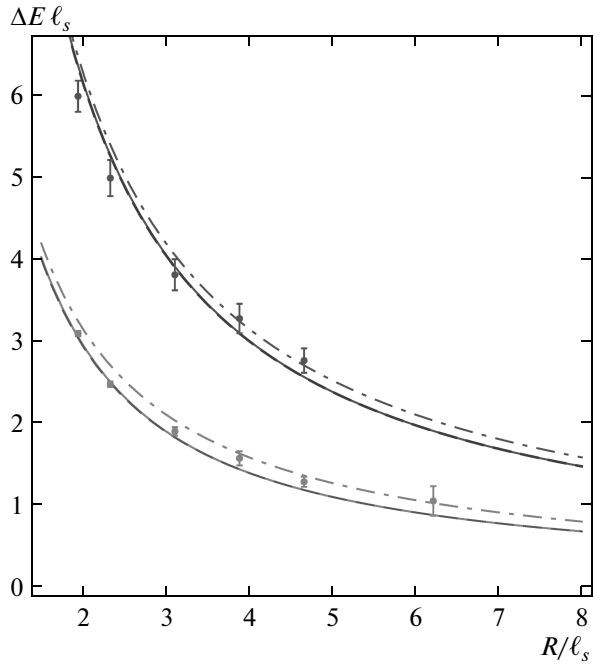

Fig. 8. $\Delta E = E - R/\ell_s^2$ as a function of the length of the flux tube for the states with left-movers with one and two units of the KK momentum in orange and red, respectively. The data is taken from [5]. The solid lines show the theoretical predictions derived from Eqs. (41)–(43) with the PS interaction taken into account to all orders. The darker dashed lines show the result in which only the GGRT phase is included. The dot-dashed line shows the ABA or in this case equivalently the free-theory result (color online [37])

the ABA result, or equivalently the free-theory answer, for the energies. The physics of these states is very simple. To a very good approximation, they are just collections of free phonons.

4.3. States with a left- and a right-mover and a new massive state

We now consider the states with one left- and one right-moving particle, each carrying one unit of momentum, i. e., $N = \tilde{N} = 1$. These are the lowest-energy states for which the ABA is nontrivial and we finally can see all ingredients of the TBA method at work. Figure 3 shows that for these states, the naive derivative expansion does not provide a good approximation for strings with lengths accessible on the lattice.

As before, keeping the GGRT part of the phase shift in the TBA system results in the GGRT expression for the energies. From Fig. 3, we find that it provides a

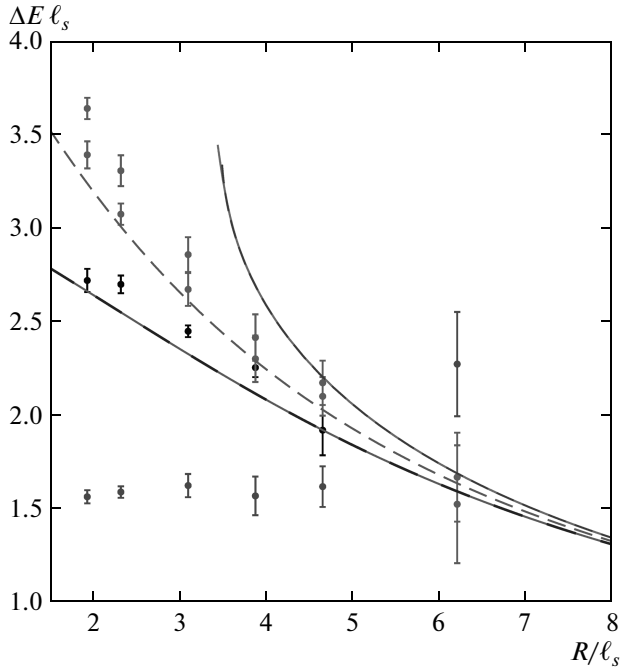

Fig. 9. $\Delta E = E - R/\ell_s^2$ as a function of the length of the flux tube for the lowest-lying states containing both left- and right-movers. The respective parity-even and parity-odd states with spin 0 are shown in blue and red. The states with spin 2 are shown in green. The data is taken from [5]. The red, blue, and lighter green lines show the theoretical predictions derived from Eqs. (41)–(43) with the PS interaction included to all orders. The darker green dashed line shows the result when both the GGRT and PS phases are taken into account in the ABA, but only the GGRT phase is taken into account for winding corrections. The two are virtually indistinguishable, once again showing the UV insensitivity of the winding corrections. The dashed gray line shows the result for the GGRT theory (color online [37])

reasonable approximation for the scalar and tensor levels, but not for the pseudoscalar. We now include the PS phase shift. Similarly to purely left-moving states, we are after four complex pseudo-energies, $\epsilon_l^{\pm}$ and $\epsilon_r^{\pm}$. They are again of the quadratic form (37) and satisfy the same reality conditions. Since our states satisfy $p_l = p_r$, the TBA system imposes the additional relation $\epsilon_l^{\pm}(q) = \epsilon_r^{\pm}(q)$ for the scalar and pseudoscalar state and $\epsilon_l^{\pm}(q) = \epsilon_r^{\mp}(q)$ for the tensor states. The resulting equations for c and d are again readily solved numerically. The results are shown in Fig. 9. The convergence of the TBA result is significantly better than that of the ℓ_s/R-expansion. For the scalar and tensor levels, we also find significantly improved agreement with the lattice data. This is noteworthy especially because so far we have not introduced any free parameter in our analysis in addition to ℓ_s, which is fixed from the ground-state data, just like in the ℓ_s/R expansion. The curves presented in Fig. 9 are therefore the results of a calculation from first principles.

The improvements in the convergence of the perturbative expansion are more prominent for the scalar state than for the tensor states. The reason for this is that in the TBA method, the perturbative approximation enters in the calculation of the scattering amplitudes. How good the perturbative expansion is, is controlled by how soft the phonon momenta $p\ell_s$ are that comprise the states. These momenta are determined from solving the TBA system and take different values in the different channels for the same value of R. The PS correction in the (pseudo)scalar channels adds to the tree-level phase shift. In the tensor channel, it has the opposite sign, and hence the phase shift grows more slowly. In agreement with the discussion at the end of Sec. 3.2, the phonon momenta are then softer in the (pseudo)scalar sectors, and therefore the perturbative expansion behaves better.

To demonstrate this effect, the theoretical curves on the plot are terminated when the momenta of the particles become large enough such that the one-loop contribution to the phase shift δ_{PS} becomes equal to the tree-level one δ_{GGRT}. This happens when $p \approx 1.8\ell_s$.

Even though the PS contribution to the phase shift affects these states significantly, its effect on the winding corrections is still negligible because the winding corrections are UV insensitive, as shown above. To illustrate this explicitly for these states, we also solved the TBA system by including the PS phase shift in the asymptotic Bethe ansatz but neglecting it in all winding contributions (i. e., in TBA constraints (13) and (14) and in the integral terms in momenta quantization conditions (11) and (12)). The result is shown in Fig. 9 together with the exact treatment. The difference is again less than 0.5 %.

The improved theoretical control makes it manifest that the anomalous behavior of the pseudoscalar level is a genuinely new physical effect and is unrelated to the bad convergence of the expansion. At this order, the scalar and pseudoscalar states, for which the expansion is well-behaved, are predicted to be degenerate. But the observed splitting between the scalar and pseudoscalar states is larger than the splitting (both predicted and observed) between the scalar and tensor states even for relatively long strings. It is then implausible to expect that this discrepancy would disap-

pear when higher-order contributions to the worldsheet S-matrix are included.

This strongly suggests that to explain the anomalous behavior of the pseudoscalar level, we need to reconsider the basic assumptions underlying our calculation and add a qualitatively new input. An important hint suggesting the missing ingredient comes from observing that the energy of the pseudoscalar level is practically independent of the length of a flux tube. This suggests that we are observing a light massive excitation on the worldsheet of a flux tube — a new particle. A similar explanation for the energy of the pseudoscalar level was suggested earlier in [5].

It is straightforward to incorporate such a state into our effective string theory framework. The minimal possibility is to introduce a new massive pseudoscalar field ϕ on the flux tube worldsheet. At the leading order in the derivative expansion, interactions of such a field with the Goldstones are described by the Lagrangian

$$\mathcal{L}_\phi = -\frac{1}{2}(\partial\phi)^2 - \frac{1}{2}m^2\phi^2 - \\ - \frac{\alpha}{8\pi}\phi\epsilon^{ij}\epsilon^{\alpha\beta}\partial_\alpha\partial_\gamma X^i\partial_\beta\partial^\gamma X^j + \dots, \quad (38)$$

where dots stand for terms that are of higher orders in fields and derivatives. In particular, these include model-independent quartic $\phi\phi XX$ couplings originating from the covariant completion of the kinetic and mass term for ϕ.

The presence of four-derivative terms in the leading pseudoscalar ϕXX coupling in (38) is dictated by nonlinearly realized Lorentz invariance. It requires that every term in the action corresponds to the expansion of some geometric invariant (see, e. g., [29] for a recent discussion). The invariant that corresponds to the interaction term in (38) is rather special and deserves some attention. It originates from

$$\nu = \frac{\alpha}{8\pi}\phi K^i_{\alpha\gamma}K^{j\gamma}_{\beta}\epsilon^{\alpha\beta}\epsilon_{ij}, \quad (39)$$

where $K^i_{\alpha\gamma}$ is the extrinsic curvature of the worldsheet. Thus, ϕ is coupled to the topological invariant known as the self-intersection number of the string worldsheet. The existence of this worldsheet θ-term for a string in a four-dimensional target-space was pointed out by Polyakov [30], and it was suggested that it should be generated on the flux tube worldsheet in the presence of the bulk θ-term [31]. Given this coupling, it is natural to refer to the field ϕ as the worldsheet axion.

This axion is not a stable particle, and it should not therefore be added to the set of asymptotic states in the TBA system. However, it does contribute to the scattering of Goldstones. In particular, it appears as a resonance in the pseudoscalar channel, where its effect is most pronounced. A diagrammatic calculation using action (38) to the leading order in α gives the contribution to the two-particle phase shift,

$$2\delta_{res}(p) = \sigma_1\frac{\alpha^2\ell_s^4p^6}{8\pi^2(4p^2+m^2)} + \\ + 2\sigma_2\tan^{-1}\left(\frac{\alpha^2\ell_s^4p^6}{8\pi^2(m^2-4p^2)}\right). \quad (40)$$

with $\sigma_1 = (-1,1,1)$, $\sigma_2 = (0,0,1)$ for the respective scalar, symmetric, and pseudoscalar channels. The σ_2-term represents the resonant s-channel contribution, while the σ_1-term arises from the t- and u-channels.

Accounting for the pseudoscalar resonance in the winding contributions is problematic because switching to the helicity field basis (30) no longer diagonalizes the full S-matrix. Already in the two-particle sector, phase shifts (40) now take different values in the scalar and pseudoscalar channels (which is, of course, the reason we introduced the resonance in the first place). As a consequence, we can no longer include the PS contribution into winding corrections. However, we have already seen that the winding corrections are not UV sensitive and that the error introduced by not including the PS contribution into the winding corrections is negligible ($\lesssim 0.5\,\%$). From now on, we therefore account for the full phase shifts only in the ABA part of the generalized momentum quantization conditions (11) and (12) and everywhere else keep only the GGRT contribution. This significantly simplifies the TBA system. The pseudo-energies become real, independent of the flavor of the particles, and linear in the momenta,

$$\epsilon^1_{l(r)}(q) = \epsilon^2_{l(r)}(q) = cq.$$

This converts the TBA equations into the simple system of algebraic equations

$$c = 1 + \frac{p\ell_s^2}{R} - \frac{\pi(D-2)}{12R^2c}\ell_s^2, \quad (41)$$

$$pR + 2\delta(p) - \frac{\pi(D-2)}{12Rc}\ell_s^2p = 2\pi N, \quad (42)$$

where $N = 1$, and the expression for the energy is

$$\Delta E = 2p - \frac{\pi(D-2)}{6Rc}. \quad (43)$$

Depending on the state, the phase shift in Eq. (42) is given by the sum of one of (32), (33) and of (40).

The axion introduces two free parameters, the mass m and the coupling α (or, equivalently, the width). We

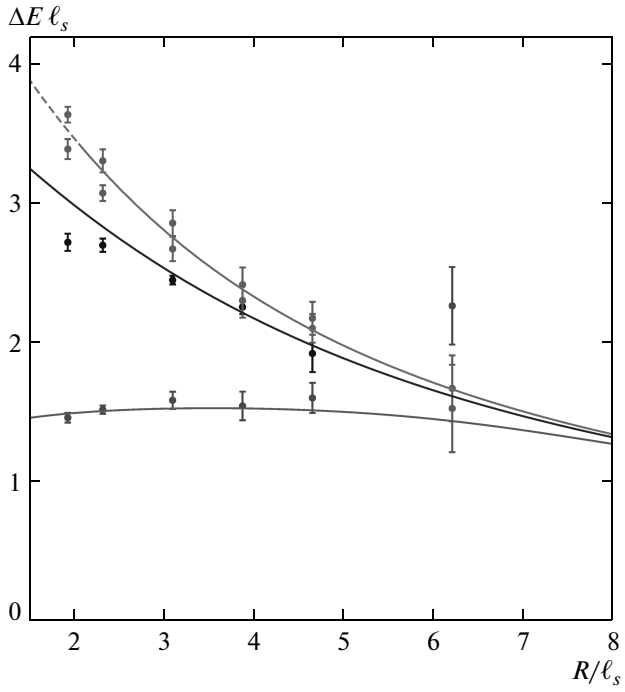

Fig. 10. $\Delta E = E - R/\ell_s^2$ as a function of the length of the flux tube for the lowest-lying states containing both left- and right-movers. The data is again taken from [5] and the coloring is as in Fig. 9. The red, blue, and green lines show the theoretical predictions derived from Eqs. (41)–(43) with the GGRT, PS, and resonance contributions to the phase shift included in the ABA, but with winding corrections only taken into account for the GGRT contribution. Lines are shown as dashed where the PS contribution becomes larger than the GGRT contribution (color online [37])

determine them by fitting the model to the data and find

$$m\ell_s = 1.85^{+0.02}_{-0.03}, \quad \alpha\ell_s^{-2} = 9.6 \pm 0.1. \tag{44}$$

In physical units, this corresponds to approximately 750 MeV, which is about a half of the mass of the lightest glueball. It should be kept in mind that the presented error bars reflect the statistical uncertainty only. We estimate the systematic errors to be comparable. The results are presented in Fig. 10. The lines on the plot become dashed where δ_{PS} becomes equal to δ_{NG}. We see that including the axion not only provided a very good fit for the pseudoscalar state but also significantly improved the fit in other channels thanks to the σ_1-term in (40). We note that changing the sign of this correction by varying the parameters is not possible, and is therefore rather nontrivial. The best fit values correspond to a relatively narrow resonance with a width equal to

$$\Gamma = 0.39/\ell_s = 0.21\, m.$$

4.4. Determination of phase shifts from the data and excited levels

Another advantage of the method developed in this paper is that it allows us to present the data in a new way. Similarly to the standard procedure used to extract scattering amplitudes from lattice calculations [19], we can use the system of equations (41)–(43) to solve for p and δ given $\Delta E(R)$. The only difference is that we include winding corrections because our phonons are massless. This alternative way of presenting data allows us to directly visualize the presence of a resonance and the extent to which the resonance improves the fit in the scalar and tensor channels. In addition, it has the advantage that we can combine different excited states in the same plot because they probe the same underlying scattering amplitudes. As an example, we consider the phase shift for the states with one left- and one right-mover as a function of the center-of-mass energy extracted from the data for the energy levels. In this case, the solution can be written in a relatively compact form

$$p_l = p_r = \frac{\Delta E}{2} + \frac{\pi}{6(\Delta E\ell_s^2 + 2R)}, \tag{45}$$

$$2\delta = 2\pi - \frac{\Delta E R}{2} + \frac{\pi}{18}\,\frac{3\Delta E^2\ell_s^4 + 2\pi\ell_s^2 - 12R^2}{(\Delta E\ell_s^2 + 2R)^2}. \tag{46}$$

The resulting phase shift as a function of momentum extracted from the data is shown in Fig. 11 along with the theoretical predictions for scattering phase shifts in various channels. We also included the data for the next excited pseudoscalar level in the lower panel. The theoretical prediction and the data still agree for the excited state at low momenta, but the agreement becomes noticeably worse as the momentum increases. Nevertheless, we clearly see the characteristic resonance shape with a mass $m \approx (1.8\text{–}1.9)\ell_s^{-1}$. The middle and upper panels of the same figure show the scalar and tensor channels, and it is clear that there is no sign of a resonance in these channels. The dashed curves represent the theory prediction in the absence of the resonance and only depend on one parameter, the string width ℓ_s. The lower panel clearly shows that a new massive pseudoscalar particle has to be introduced to explain the data.

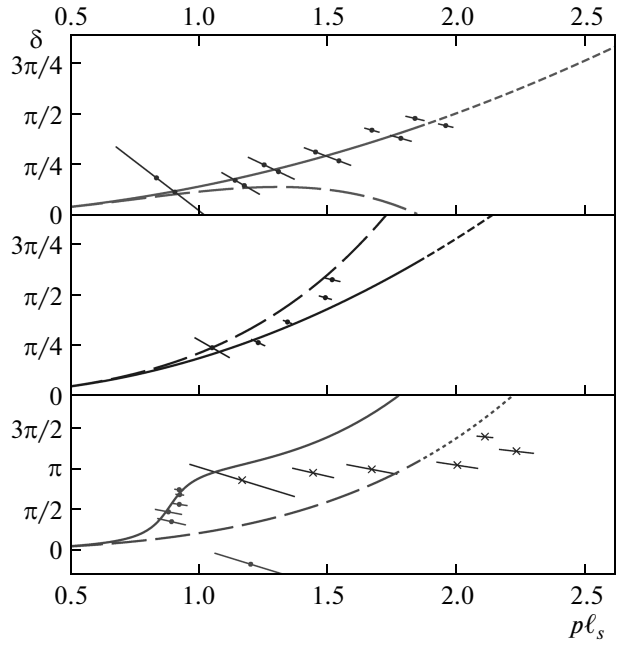

Fig. 11. The scattering phase shift δ for two Goldstone bosons as a function of the center-of-mass momentum in the symmetric traceless, scalar, and antisymmetric channel in the respective top, middle, and bottom panels. The solid and the long dashed lines respectively show the theoretical prediction with and without the worldsheet axion

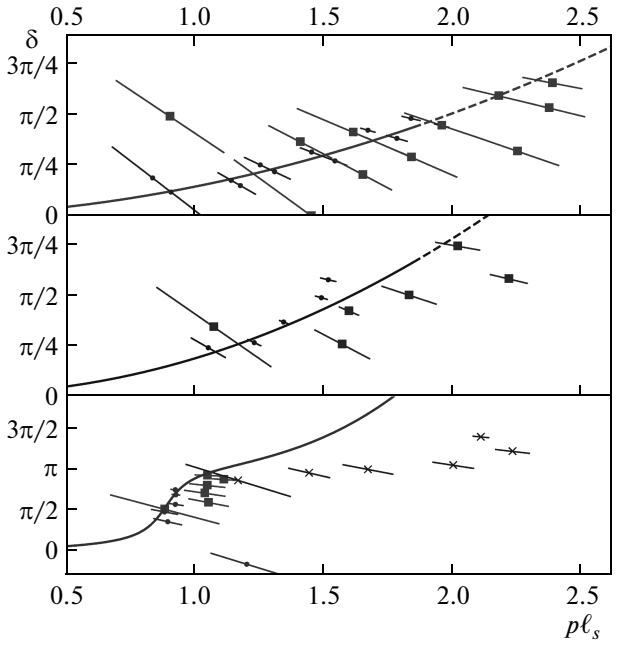

Fig. 12. The scattering phase shift δ for two Goldstone bosons as a function of the center-of-mass momentum in the symmetric traceless, scalar, and antisymmetric channel in the respective top, middle, and bottom panels. The darker points show the lowest-lying states with zero total momentum, the crosses show the first excited pseudoscalar state, and the squares show the lowest-lying states with one unit of total momentum. The lines show the theoretical prediction

Of course, introducing a new massive pseudoscalar state leads to additional predictions. As already mentioned, it also affects the scalar and tensor states and improves the agreement between theory and lattice data for them. In addition, we should be able to give momentum to this particle so as to make definite predictions for excited states with a nonzero total momentum, for which data is also available. If we extract phase shifts from the data for excited states with one left- and one right-mover with unequal momenta, we expect to find a resonance there as well. We show the result for the state in which the left-mover has one and the right-mover has two units of the KK momentum in Fig. 12, together with the theoretical prediction and the data for the state with zero total momentum, which we discussed above. Similarly, predictions can be made for the scalar and tensor states with a nonzero total momentum. The states with one unit of the total momentum for scalars and tensors are also shown in Fig. 12. The phase shifts extracted from the different excited states agree relatively well, almost within the statistical errors of the lattice calculations. In particular, we do see the resonance not only in the state with the total momentum zero but also in the state with a nonzero momentum. The small discrepancy between the two can be attributed to two effects. We did not include the finite-size corrections due to the resonance itself into our calculation. An estimate shows that this affects the data points corresponding to the shortest lengths more strongly (as one would expect), and brings the phase shifts from the state with the total momentum zero and unity into slightly better agreement. The remaining difference seems to be due to discretization effects in the lattice calculations themselves, which are also responsible for the splitting between the two tensor states.

4.5. $D = 3$ Yang–Mills

These techniques can, of course, be also applied to the existing lattice data in $D = 3$ dimensions. In this case, we have a single channel for two-particle scattering. The nonlinearly realized Lorentz invariance implies that the phase shift takes the form

$$2\delta = 2\delta_{GGRT} + \mathcal{O}(\ell_s^6 s^3). \quad (47)$$

The corrections here are nonuniversal. In particular, as already mentioned, the GGRT phase shift itself is compatible with nonlinearly realized Lorentz symmetry for $D = 3$.

In this section, we compare the data from [6], which is for the gauge group $SU(6)$ with $\beta = 171$ and the Wilson loop in the fundamental representation, with the GGRT prediction. The result for the five lowest-lying states with an even number of phonons and zero total momentum is shown in Fig. 13. We see that all states are in qualitative agreement with the GGRT phase shift and see no evidence for new light massive states. However, there are small quantitative differences between the GGRT prediction and the data. The energies of the states shown in yellow and orange correspond to states with two and four phonons and are predicted to be degenerate. However, they appear to be split in the data. Furthermore, the measured energies are systematically below the GGRT prediction. This suggests that the binding energy between the phonons is larger in the $SU(6)$ gauge theory than in the GGRT theory, which implies a phase shift that grows more rapidly, consistently with what is seen in the right panel of Fig. 13. It is then natural to introduce corrections into the phase shift

$$2\delta = 2\delta_{GGRT} + \gamma_3 \ell_s^6 s^3, \quad (48)$$

and determine this leading correction from the data using the TBA, taking only the GGRT phase shift in the windings into account, as before. Such a correction to the phase shift would follow from higher-order geometric invariants in the Goldstone theory such as R^2 in the action, and we can trust our procedure provided the coefficient is small enough, such that this is in fact a correction for the range of momenta of interest. Based on loop counting, we expect the coefficient to be of the order $1/(2\pi)^2$, which should roughly be reliable for $p\ell_s \lesssim \sqrt{2\pi}$, including all data points of the first excited state for both two- and four-particle states, but only some of the second excited two-particle state. We extract γ_3 from the first excited two-particle state using the TBA equations (41)–(43) as well as the first excited four-particle state using the relations

$$c = 1 + 2\frac{p\ell_s^2}{R} - \frac{\pi(D-2)}{12R^2 c}\ell_s^2, \quad (49)$$

$$pR + 4\delta(p) - \frac{\pi(D-2)}{12Rc}\ell_s^2 p = 2\pi N \quad (50)$$

with $N = 1$, and

$$\Delta E = 4p - \frac{\pi(D-2)}{6Rc}. \quad (51)$$

Including all data points with $p\ell_s \leq 2$ and taking the error bars at face value, we find

$$\gamma_3 = \frac{0.7 \pm 0.1}{(2\pi)^2}, \quad (52)$$

nonzero at approximately 7σ. This correction increases the binding energies and thus lowers the energies of the theory prediction. It also introduces a splitting between two-particle states and four-particle states, in agreement with the data simply because the phonons comprising the two-particle states carry larger momenta and are more strongly bound than the phonons making up the four-particle states.

Ignoring the contributions to the winding corrections from corrections to the GGRT phase shift has so far worked well. There is a subtlety, however. The positive coefficient γ_3 implies a correction to the pseudo-energies with a negative coefficient. As a consequence, the integrals in the TBA equations are no longer convergent. These divergences are not surprising and arise because higher-derivative theories typically come with ghosts around the cut-off scale. The perturbative calculation presented in Sec. 3.3 shows that this happens for positive γ_3. We know, of course, that the full theory does not have ghosts and that there are higher-order terms that cure the divergences. Introducing such higher-order terms by hand seems unsatisfactory because it would introduce additional arbitrary coefficients. It seems more appealing to interptret the $\ell_s^6 s^3$ correction as arising from a heavy resonance that has been integrated out, which suggests the phase shift

$$\exp(2i\delta) = \exp(2i\tilde{\ell}_s^2 p_l p_r)\frac{s - 2iM\Gamma + M^2}{s + 2iM\Gamma + M^2} \times \times \frac{s - 2iM\Gamma - M^2}{s + 2iM\Gamma - M^2}, \quad (53)$$

where

$$\tilde{\ell}_s^2 = \ell_s^2 - \frac{32\Gamma}{M(M^2 + 4\Gamma^2)}, \quad (54)$$

whence the correct phase shift is recovered for $s \ll M^2$. This amplitude (53) is not consistent with the nonlinearly realized symmetries and should for now be simply thought of as a fitting function that has the desirable property that the integrals in the TBA remain finite and corrections to windings relative to those in the GGRT theory remain small. Fitting to the data, we find

$$M = 3.7/\ell_s \quad \text{and} \quad \Gamma = 1.0/\ell_s. \quad (55)$$

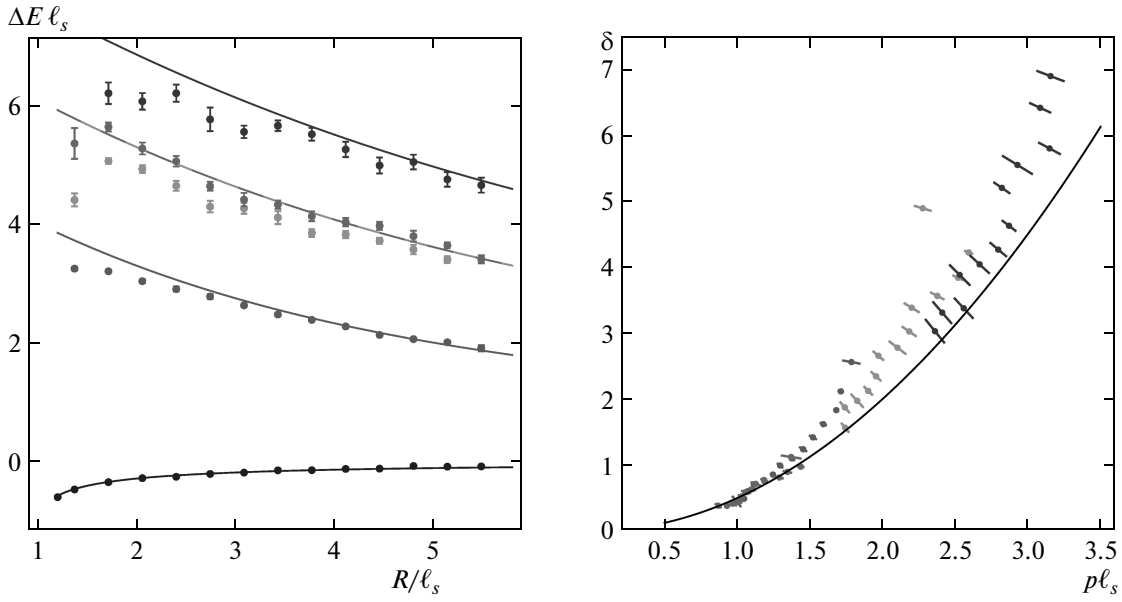

Fig. 13. The energy and scattering phase shift δ for the lowest-lying parity-even states with zero total momentum. The lines show the theoretical prediction of the GGRT theory (color online [37])

Upon expansion in s, this leads to a value of γ_3 in good agreement with Eq. (52), and hence the phase shift is approximated well by our fitting function below the resonance. Above the resonance, it does not have the correct behavior compatible with the nonlinearly realized Lorentz invariance and should therefore not be trusted for $p\ell_s > 1.85$.

The resulting predictions for the energy levels of the states involved in the fit are shown in Fig. 14, and we see that the modified phase shift correctly reproduces the larger binding energies and the splitting between two- and four-particle states seen in the data. The momenta for some of the data points for the second excited two-particle state as well as the data points for the third excited two-particle state are so large that our approximations become unreliable. The ground state, however, is rather insensitive to the UV behavior of the phase shift, and it is interesting to compute the correction to the ground-state energy that corresponds to our correction to the phase shift. We do this by solving the TBA numerically by iterations. The result is shown in Fig. 15. The left panel shows that the ground-state data is in good agreement with our prediction. The right panel shows that the leading correction to the GGRT ground state energy is well described by an R^{-7} term down to $R > 1.5\ell_s$ and becomes as steep as R^{-11} for the shortest strings studied in [6].

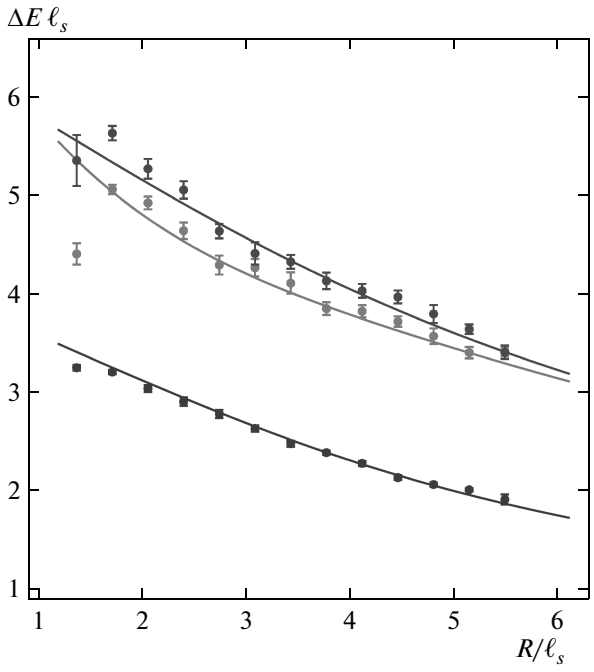

Fig. 14. The energies of the states included in the fit for the correction to the scattering phase shift at the order ℓ_s^6. The lines show the theoretical prediction. For the second excited two-particle state, only data for six longest strings is included in the fit because the phonon momenta become too large

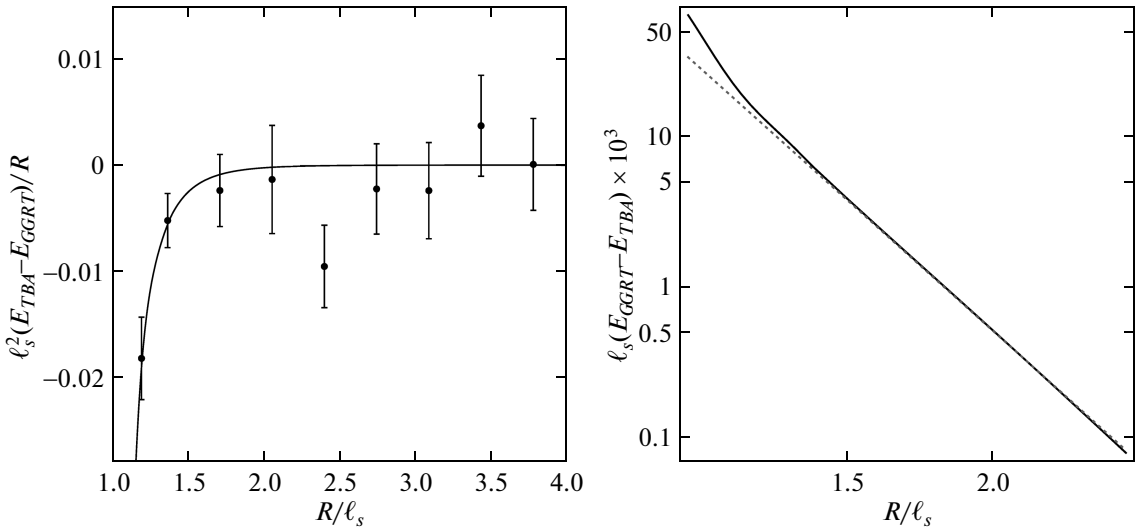

Fig. 15. The left panel shows the ground-state energy predicted from the fit of the phase shift to the excited states relative to the GGRT prediction. The right panel shows a log–log plot illustrating that the correction for $R > 1.5\ell_s$ behaves as R^{-7} and becomes as steep as R^{-11} for smaller R

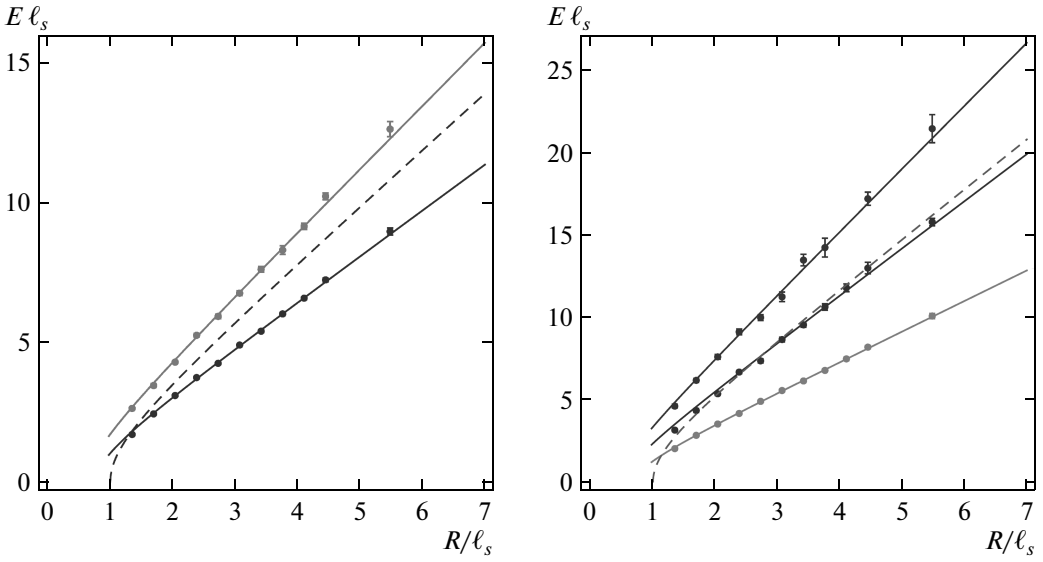

Fig. 16. The energies of the ground states for k-strings with $k = 2$ (left) and $k = 3$ (right). For $k = 2$, the data for the antisymmetric and symmetric representations of $SU(6)$ are shown in green and yellow. For $k = 3$, we show the data for the antisymmetric, mixed, and symmetric representations in orange, red, and purple. The solid lines represent the GGRT prediction with the tension derived from a fit to the data as before. The dashed lines show the energy for the state with the same charge under the center group consisting of noninteracting fundamental strings (color online [37])

4.6. k-strings in $D = 3$ Yang–Mills

In addition to the data for Wilson loops in the fundamental representation presented in [6], nice data for $SU(6)$ gauge group at $\beta = 171$ has recently been presented for bound states of such strings with $k = 2$ and $k = 3$ units of charge under the center symmetry [7]. The left panel of Fig. 16 shows the data for the ground states with $k = 2$ in the antisymmetric and symmetric representation together with the GGRT prediction.

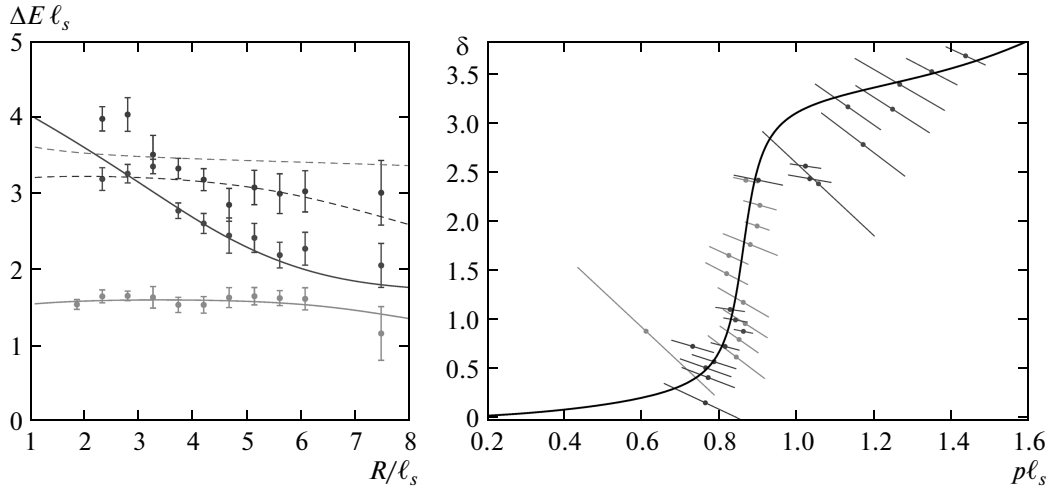

Fig. 17. The left panel shows the energy as a function of the string length for the lowest-lying excited states for the antisymmetric representation with $k = 3$ with an even number of phonons and zero total momentum. The solid lines are the theory predictions for the 2-particle states, dashed lines represent 4-particle states. The right panel shows the phase shift extracted from the data (color online [37])

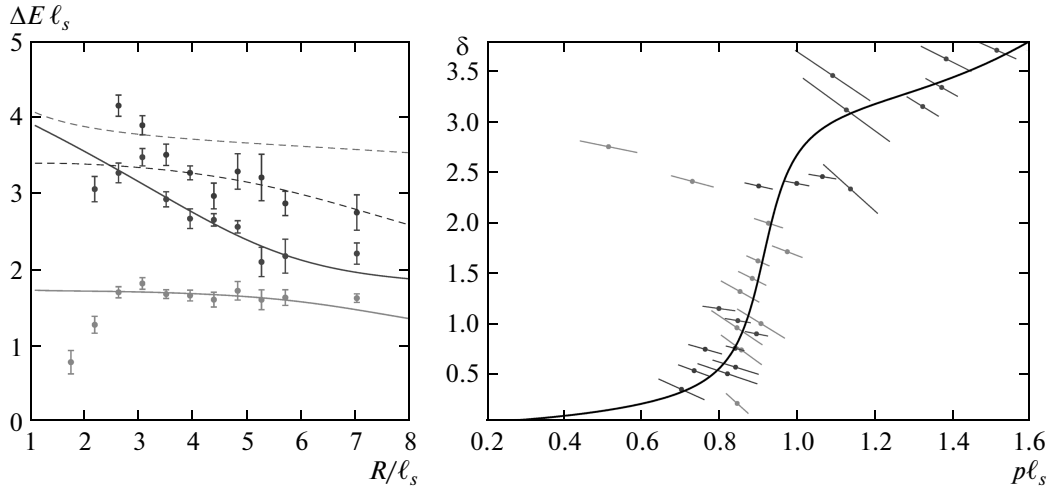

Fig. 18. The left panel shows the energy as a function of the string length for the lowest-lying excited states for the antisymmetric representation with $k = 2$ with an even number of phonons and zero total momentum. The solid lines are the theory predictions for the 2-particle states, the dashed lines represent 4-particle states. The right panel shows the phase shift extracted from the data (color online [37])

The right panel of Fig. 16 shows the ground-state data for the antisymmetric, mixed, and symmetric representations with $k = 3$. Higher representations are related to these by charge conjugation. For comparison, we also show the energies corresponding to two and three noninteracting fundamental strings as dashed lines. An analytic calculation of the tension of these objects that is in remarkable agreement with the numerical data can be found in [32]. The antisymmetric representations are bound for both $k = 2$ and $k = 3$. The symmetric representations are unbound for both $k = 2$ and $k = = 3$, while the mixed representation for $k = 3$ is at best marginally bound. This motivates us to study the antisymmetric representations in more detail and leave the others for a future study. To illustrate that our methods also work for k-strings, we show the energy

levels and phase shift for the states with equal numbers of left- and right-movers and zero total momentum in Figs. 17 and 18, extracting phase shifts for 2- and 4-particle states using Eqs. (41)–(43) and (49)–(51). The data shows clear evidence for a resonance and the theory predictions are obtained with the resonance with

$$m = 1.88/\ell_s^{2A} \text{ and } \Gamma = 0.29/\ell_s^{2A}, \tag{56}$$

$$m = 1.74/\ell_s^{3A} \text{ and } \Gamma = 0.16/\ell_s^{3A}, \tag{57}$$

where the superscript denotes the representation of the string. It was perhaps natural to expect the presence of resonances for k-strings, given that these can be thought of as bound states of two fundamental flux tubes. It is intriguing that the values for the mass and the width are close when measured in the corresponding string units (and close to the mass and width of the worldsheet axion in $4D$).

These states nicely illustrate that the energy plots can be rather complex because of level crossing even with a very simple phase shift. The solid lines represent the theory predictions for 2-particle states, the dashed lines those for 4-particle states. We clearly see avoided level crossing for the 2-particle states as well as between the 4-particle states. However, the 2- and 4-particle states, shown in red and purple, cross. In the integrable theory, these states have different quantum numbers and do not mix. In QCD, the integrability is not exact and a certain amount of mixing between 2- and 4-particle states is expected, which would lead to avoided level crossing.

The theory predictions also show that the extraction of these energy levels is very subtle because several energy levels have comparable energies and the correlation function may not be dominated by a single exponential. Also, the phase shift extraction from the energy levels in the region of level crossing is not completely straightforward due to ambiguities of quantum number assignments. The identification of two- and four-particle states employed here appears to produce the most meaningful results on the phase shift plot, but we cannot exclude at the moment that some of the data points might have been misidentified, especially for $k = 2$ strings. This motivates further high-precision lattice measurements of these states. Hopefully, techniques presented here might be helpful in guiding these measurements.

We note an interesting feature exhibited by the $k = 2$ data: a very pronounced break in the resonance plateau on the energy plot for the lowest (orange) level at $R/\ell_s^{2A} \lesssim 3$. The corresponding points also show up very far from the theory curve on the corresponding phase shift plot. The natural explanation for the origin of this break is that it occurs when the physical size of the compact dimension becomes comparable to the size of the massive resonant state. Our phase shift extraction becomes unreliable at these short radii, because the winding corrections due to the resonance become large. This interpretation is supported by observing that a very similar break at the same values of R also appears in the lightest glueball energy plot [7], suggesting that the size of the resonance is roughly equal to the size of the lightest glueball.

The $k = 3$ data does not exhibit such a break. Perhaps only the shortest point in Fig. 17 (with $R/\ell_s^{3A} \approx \approx 2$) can be considered an indication for the beginning of the break. This is in agreement with the $k = 3$ string being much more strongly bound than the $k = 2$ strings. The $k = 3$ tension is equal to $\sigma_{3A} \approx 0.6 \cdot 3\sigma_f$, while the $k = 2$ tension is $\sigma_{2A} \approx 0.8 \cdot 2\sigma_f$, where σ_f is the fundamental flux tube tension.

5. FUTURE DIRECTIONS AND CONCLUSIONS

We feel that the most important conclusion to be drawn from this paper is that there is strong motivation for further high-precision lattice studies of the properties of flux tubes. The TBA method provides a solid analytic framework for theoretical interpretation of lattice results for the flux tube lengths that are accessible with the existing computer power. This opens the possibility for a comprehensive description of the worldsheet dynamics of the confining strings in the near future, which might be an important step towards understanding the physics of confinement.

The results presented here pose a number of intriguing questions, which may be answered with a new data. Many of them concern the nature of the observed pseudoscalar resonance in the $D = 4$ data. In particular, the phase shift plots in Figs. 11 and 12 show a systematic disagreement between the theory curve and the data at the momenta above the resonance in the pseudoscalar channel. By itself, this disagreement is not very dramatic, given that the corresponding momenta are already quite large. But an intriguing property of the observed phase shift in the pseudoscalar channel is a pronounced plateau at $\delta \approx \pi$, which corresponds to the absence of scattering. Together with a systematically better agreement between theory and data in other channels, this suggests that some interesting pieces of physics may still be missing.

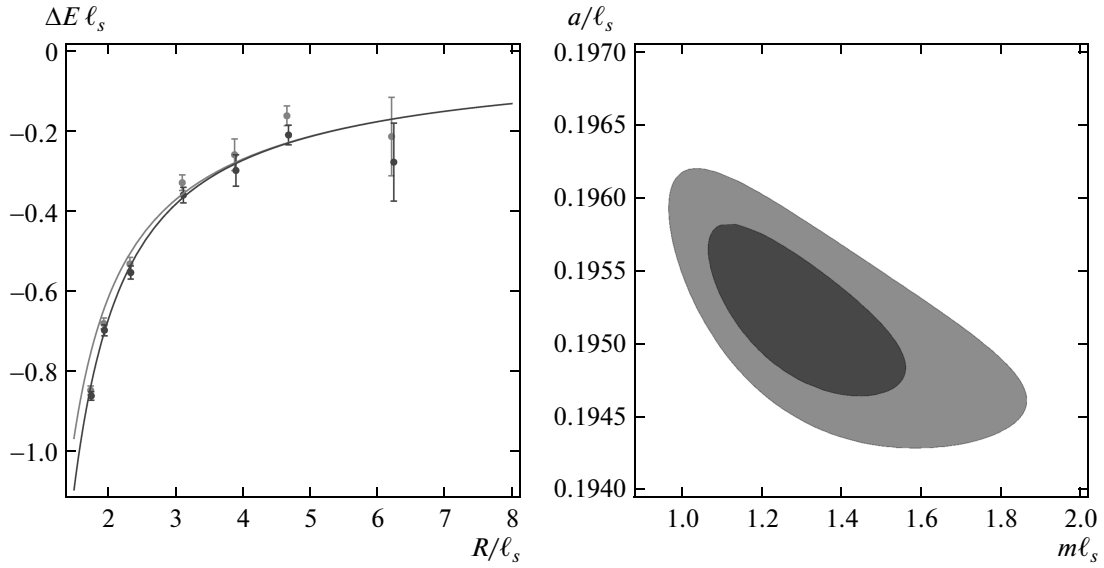

Fig. 19. The left panel shows the ground-state energy in the absence and presence of additional massive states in lighter and darker green, respectively. The data points shift because we simultaneously fit for the mass and the string tension. The right panel shows the one- and two-sigma contours in the mass–tension plane. The shortest point was not included in the fit, but nevertheless fits well (color online [37])

The experience with $D = 3$ k-string data suggests that (at least partially) the plateau may be an artifact resulting from misidentification of the excited-state data points. The phase shift plot was constructed assuming that these correspond to the two-particle state. It appears very likely that some of these points (in particular, those with $p\ell_s \gtrsim 2$) represent a four-particle state instead. With this interpretation, the deduced values of the momenta will be roughly halved, bringing these points into the resonance region and significantly decreasing the tension between theory and data. Resolving this question will require both more accurate data for excited states in this region and further theoretical work. Indeed, including four-particle states in the analysis is not as straightforward for $D = 4$ data as it was in $D = 3$ due to a larger number of channels in $D = 4$. There is no problem of principle here, and we plan to implement this in future work.

The plateau may be indicative of even more interesting physics. Indeed, the axion model in (38) represents only a minimal effective field theory explaining the observed resonance in the pseudoscalar channel. More complicated scenarios are possible. In particular, we note that as a consequence of two-dimensional kinematics, a two-particle threshold generically appears as a resonant pole. This opens an interesting possibility that the axion may in fact be a threshold bound state of even lighter massive worldsheet excitations.

Even if this possibility is not realized, it is a well-motivated question whether the axion is indeed the lightest massive mode, or there might be lighter massive states missed by the lattice searches. For an insight into how light these states might be, we can use the available high precision data for the ground-state energy. A free particle of a mass m on the worldsheet results in an additional contribution to the ground-state Casimir energy of the form

$$\Delta E(R) = -\frac{m}{\pi}\sum_n \frac{1}{n} K_1(mnR).$$

Given that the lattice data shows no sign of a resonance in the scalar channel, we consider the effect of adding a pair of such particles on the ground-state energy (having a massive $O(2)$ vector in mind). The result is presented in Fig. 19. We exclude the data point corresponding to the shortest string from the fit to be conservative. We see that the best-fit value for the mass is $m \approx 1.3\ell_s$. Taking the error bars at face value, we find an improvement in the fit corresponding to almost 4σ (and much larger if the data for the shortest string had been included) in favor of the existence of additional light particles.

A comparable improvement of the fit may be achieved by adding an R^{-7} correction to the gro-

und-state energy, but the required value for the corresponding coefficient is about a factor of five larger than the typical size of the loop corrections (estimated from the expansion of the GGRT ground-state energy).

Of course, these considerations do not take possible lattice systematics into account. Most of the improvement in the fit is driven by the data points corresponding to the shortest strings, which might suffer from possible discretization effects and from their proximity to the deconfinement transition. Nevertheless, this observation provides an additional strong motivation for the systematic search for "exotic" light states on the worldsheet with quantum numbers for which the corresponding NG state is expected to be heavy.

The natural candidate operators for creating new massive states on the worldsheet are Polyakov loops with additional local insertions, such as

$$W_{\mu\nu} = \mathrm{Tr}\, P \left(F_{\mu\nu} \exp \int\limits_C A \right). \qquad (58)$$

It is intriguing that the basis of operators used in [5] includes such an operator with $(\mu\nu)$ indices in the transverse plane (i. e., a pseudoscalar), but not with other orientations. Related to this, to understand the origin of the worldsheet axion better it will be interesting to study which operator provides the best overlap for the corresponding state, with (58) providing the most natural candidate.

It would be very interesting to understand the microscopic origin of the worldsheet axion, i. e., to derive it from the 4D QCD description. We note in this respect that a pseudoscalar state with the same mass (in string units) is also present in the available $SU(5)$ data from [5], and hence the axion appears to be present in the large N limit. Unfortunately, however, it appears impossible to use holographic gravitational AdS/QCD models to look for the axion quantitatively. For the gravitational description to be applicable, the string length should be short compared to the AdS curvature length. This implies that the mass of the light glueballs (gravitational KK modes) is parametrically smaller than the confining string tension, which is not the appropriate regime to describe the pure glue theory.

A less ambitious goal would be to look for footprints of the worldsheet axion in the spectrum of $4D$ states. This should be possible, given that there is no fundamental obstacle for extending the TBA technique to open strings. First steps in this direction have already been taken in [33] (see also [34], where the effect of the PS interaction on the open string spectrum was discussed using the conformal gauge approach). Assuming that the worldsheet axion survives in the presence of quarks, this opens an exciting possibility to see its presence in the physical spectrum of mesons. In particular, we may expect mesons with a sufficiently high spin (such that the corresponding flux tube is long enough) to exhibit universal excitations with energy of the order of the axion mass 750 MeV and of the opposite parity, corresponding to an addition of the axion to the confining flux tube. This expectation appears to be supported by the available lattice data for open strings in $SU(3)$ gluodynamics [35], which shows an anomalous Σ_u^- excitation with the energy that matches the worldsheet axion mass well, as was previously pointed out in [36].

We are especially grateful to Mike Teper for many useful discussions and for providing us with the lattice data in electronic form. We thank Ofer Aharony, Giga Gabadadze, Simeon Hellerman, Zohar Komargodski, Mehrdad Mirbabayi, Joe Polchinski, Massimo Porrati, Matt Roberts, Misha Shifman, Arkady Tseytlin, Gabriele Veneziano, and Giovanni Villadoro for the useful discussions and feedback. This work is supported in part by the NSF under grant numbers PHY-1068438 as well as PHY-1316452. One of the authors (R. F.) gratefully acknowledges the Raymond and Beverly Sackler Foundation for their support. R. F. is also supported in part by the NSF grants PHY-1213563 and PHY-0645435.

REFERENCES

1. G. Veneziano, Nuovo Cim. A **57**, 190 (1968).
2. F. Bissey, F.-G. Cao, A. Kitson et al., Phys. Rev. D **76**, 114512 (2007), arXiv:hep-lat/0606016.
3. J. M. Maldacena, Adv. Theor. Math. Phys. **2**, 231 (1998), arXiv:hep-th/9711200.
4. A. M. Polyakov, Int. J. Mod. Phys. A **14**, 645 (1999), arXiv:hep-th/9809057.
5. A. Athenodorou, B. Bringoltz, and M. Teper, JHEP **1102**, 030 (2011), arXiv:1007.4720.
6. A. Athenodorou, B. Bringoltz, and M. Teper, JHEP **1105**, 042 (2011), arXiv:1103.5854.
7. A. Athenodorou and M. Teper, JHEP **1306**, 053 (2013), arXiv:1303.5946.
8. M. Lüscher, Nucl. Phys. B **180**, 317 (1981).
9. M. Lüscher and P. Weisz, JHEP **0407**, 014 (2004), arXiv:hep-th/0406205.

10. O. Aharony and N. Klinghoffer, JHEP **1012**, 058 (2010), arXiv:1008.2648.

11. P. Goddard, J. Goldstone, C. Rebbi, and C. B. Thorn, Nucl. Phys. B **56**, 109 (1973).

12. J. Arvis, Phys. Lett. B **127**, 106 (1983).

13. S. Dubovsky, R. Flauger, and V. Gorbenko, Phys. Rev. Lett. **111**, 062006 (2013), arXiv:1301.2325.

14. O. Aharony and Z. Komargodski, JHEP **1305**, 118 (2013), arXiv:1302.6257.

15. S. Dubovsky, R. Flauger, and V. Gorbenko, JHEP **1209**, 044 (2012), arXiv:1203.1054.

16. A. Zamolodchikov, Nucl. Phys. B **342**, 695 (1990).

17. P. Dorey and R. Tateo, Nucl. Phys. B **482**, 639 (1996), arXiv:hep-th/9607167.

18. M. Lüscher, Comm. Math. Phys. **104**, 177 (1986).

19. M. Lüscher, Comm. Math. Phys. **105**, 153 (1986).

20. B. Lucini and M. Panero, Phys. Rep. **526**, 93 (2013), arXiv:1210.4997.

21. L. Mezincescu and P. K. Townsend, Phys. Rev. Lett. **105**, 191601 (2010), arXiv:1008.2334.

22. S. Dubovsky, R. Flauger, and V. Gorbenko, JHEP **1209**, 133 (2012), arXiv:1205.6805.

23. J. Polchinski and A. Strominger, Phys. Rev. Lett. **67**, 1681 (1991).

24. O. Aharony, M. Field, and N. Klinghoffer, JHEP **1204**, 048 (2012), arXiv:1111.5757.

25. M. T. Hansen and S. R. Sharpe, Phys. Rev. D **86**, 016007 (2012), arXiv:1204.0826.

26. M. T. Hansen and S. R. Sharpe, arXiv:1311.4848.

27. J. Teschner, Nucl. Phys. B **799**, 403 (2008), arXiv: hep-th/0702214.

28. R. A. Janik, Lett. Math. Phys. **99**, 277 (2012), arXiv: 1012.3994.

29. P. Cooper, Phys. Rev. D **88**, 025047 (2013), arXiv: 1303.0743.

30. A. M. Polyakov, Nucl. Phys. B **268**, 406 (1986).

31. P. Mazur and V. Nair, Nucl. Phys. B **284**, 146 (1987).

32. D. Karabali and V. Nair, Phys. Rev. D **77**, 025014 (2008), arXiv:0705.2898.

33. M. Caselle, D. Fioravanti, F. Gliozzi, and R. Tateo, JHEP **1307**, 071 (2013), arXiv:1305.1278.

34. S. Hellerman and I. Swanson, arXiv:1312.0999.

35. K. J. Juge, J. Kuti, and C. Morningstar, Phys. Rev. Lett. **90**, 161601 (2003), arXiv:hep-lat/0207004.

36. O. Andreev, Phys. Rev. D **86**, 065013 (2012), arXiv: 1207.1892.

37. S. Dubovsky, R. Flauger, and V. Gorbenko, arXiv: 1404.0037v1.